Eur. Phys. J. D **37**, 1–21 (2006)
DOI: 10.1140/epjd/e2005-00249-7

THE EUROPEAN PHYSICAL JOURNAL D

New FTS measurements, optimized energy levels and refined VUV standards in the Ne III spectrum*

A.E. Kramida[a] and G. Nave

National Institute of Standards and Technology, Gaithersburg, MD 20899, USA

Received 14 March 2005 / Received in final form 28 June 2005
Published online 6 September 2005

Abstract. All observed spectral lines of Ne III in the range 204 Å to 36 μm (277 cm^{-1} to 490000 cm^{-1}) have been compiled and critically evaluated. 57 visible and ultraviolet lines of Ne III have been precisely measured using Fourier transform spectroscopy. An optimized level scheme has been derived from the total list of observed lines. Relative positions of about 180 out of a total of 226 previously known energy levels of Ne III have been determined with improved accuracy compared to previous studies. Excitation energies of almost all excited levels have been revised by (1.5–2.0) cm^{-1}. 127 precise wavelength standards in the region 210 Å to 2900 Å have been derived. Concepts of *error current* and *covariance matrix* have been implemented in a computational algorithm that permits one to derive the uncertainties of Ritz wavelength standards obtained from a set of least-squares-optimized energy levels. Nine new energy levels have been found, and 16 new transitions have been identified in the extreme ultraviolet region. The ionization potential has been increased by 4.5 cm^{-1}. The new value is (511543.5 ± 2.7) cm^{-1} (63.4233 eV ± 0.0003 eV).

PACS. 32.10.Fn Fine and hyperfine structure – 32.10.Hq Ionization potentials, electron affinities – 32.30.Jc Visible and ultraviolet spectra – 32.70.Cs Oscillator strengths, lifetimes, transition moments – 31.15.Ct Semi-empirical and empirical calculations (differential overlap, Hückel, PPP methods, etc.) – 95.30.Ky Atomic and molecular data, spectra, and spectral parameters (opacities, rotation constants, line identification, oscillator strengths, gf values, transition probabilities, etc.)

1 Introduction

The spectrum of doubly ionized neon was first analyzed by de Bruin in 1932 [1], von Keussler in 1933 [2] and Boyce in 1934 [3]. These works were used by Moore in her compilation [4]. Since then, Bowen in 1955 [5] and 1960 [6] measured three very important parity-forbidden Ne III lines in emission spectra of planetary nebulae. In 1971, Persson [7] made an important advance in the laboratory investigation of the spectrum. He used a hollow cathode discharge to analyze the Ne II lines in the visible and ultraviolet (UV) regions with much higher precision than earlier. The low intensity of the Ne III lines did not permit him to make a complete analysis of this spectrum, but he published the energy values for the levels of the Ne III ground configuration derived from Bowen's data [5] along with the values he deduced from his Ne II line series measurements. In 1980, Edlén used the Ne III levels from Persson [7] in his compilation of the levels of the $2s^2 2p^4$ configuration along the O I sequence [8].

The most complete analysis of the Ne III spectrum was published by Persson et al. in 1991 [9]. A comprehensive review of all experimental studies of the Ne III spectrum in the period 1969 through 1990 can be found in this paper. Persson et al. [9] combined the earlier accurate measurements of a hollow cathode spectrum [7] with a less accurate but more intense spectrum from a theta pinch. As a result, they succeeded in making a number of new identifications and deriving the most complete level system. However, their list of energy levels has some deficiencies. First of all, the forbidden transitions observed by Bowen [5,6] were not included in the procedure of level optimization. As a result, the levels of the $2s^2 2p^4$ configuration listed in [9] disagree with those from [7] (which we consider to be more accurate) by 0.5 cm^{-1} to 1.5 cm^{-1}. This leads to displacement of the same order of magnitude for most of the upper levels. In addition, our analysis showed that some of the levels given in [9] were not optimized against the whole set of observed transitions listed in the same paper. These considerations provide a sufficient reason to revise the list of levels in reference [9]. In addition, new precise measurements of more than 100 wavelengths in the vacuum ultraviolet (VUV), UV, visible, and infrared regions [10–12] have become available. In particular, the forbidden $2p^4\ {}^3\mathrm{P}_1 - {}^3\mathrm{P}_0$ and ${}^3\mathrm{P}_2 - {}^3\mathrm{P}_1$ infrared lines were interferometrically measured by Feuchtgruber et al. [11] with an unprecedented accuracy of 0.0003 μm in observed spectra of astronomical objects. Several lines that were masked in the spectrum recorded by Persson et al. [9] have been

* The full version of Table 2 is only available in electronic form at `http://www.eurphysj.org`

[a] e-mail: `Alexander.Kramida@nist.gov`

resolved in spectra of platinum-neon discharges observed by Sansonetti et al. [10] and in the iron-neon hollow cathode spectrum measured by means of Fourier transform spectroscopy (FTS) in the present work. In particular, three combinations involving the $2s^2 2p^3(^2\mathrm{P}^\circ)4s\ ^3\mathrm{P}^\circ_0$ level have been resolved which were either masked or blended in Persson's spectrum. This permitted us to determine the positions of the levels involved more accurately. For example, the displacement of the $2s^2 2p^3(^2\mathrm{P}^\circ)4s\ ^3\mathrm{P}^\circ_0$ level is about 6 cm^{-1} compared to Persson's position [9]. Brosius et al. [12] used a hollow cathode lamp to excite the extreme ultraviolet (EUV) spectrum of neon and re-measured several Ne III lines against the Ritz standard wavelengths of Ne II and He II lines. Their measurements significantly reduce the uncertainties of the energies of the excited configurations relative to the ground state.

Apart from these improved line measurements, the observed Ne III spectrum was extended in the extreme ultraviolet (EUV) region by Livingston et al. [13]. Independently, Bastin [14] has found that some of the EUV lines ascribed to Ne IV by Paul and Polster [15] actually correspond to transitions between known levels of Ne III. His new assignments of these lines are completely consistent with identifications of Livingston et al. [13]. Most of the Ne III lines observed in [13] have been identified as transitions between known levels, although some of the lines were tentatively ascribed to newly found levels. A special set of calculations by means of Cowan's code [22] performed in the present work has confirmed some of the tentative assignments made in [13] and yielded a few new ones.

The main purpose of the present paper is to obtain more accurate energy levels of Ne III by means of an optimization procedure that takes into account the whole extended set of observed lines, including those that were precisely measured in our Fourier-transform (FT) spectra, and from these more accurate levels to derive new wavelength standards in the VUV region.

2 New FTS measurements

The FT spectra used in the present investigation were the same as those used in the studies of the Fe II spectrum [16]. Two different spectrometers were used: the $f/60$ IR–visible–UV FT spectrometer at the National Solar Observatory, Tucson, Arizona, for the region above 2800 Å; and the $f/25$ VUV FT spectrometer at Imperial College, for the region 1500 Å to 3100 Å. The light source was a high-current hollow cathode of pure iron run in 100 Pa to 500 Pa (0.5 Torr to 4 Torr) of neon with dc currents of 0.32 A to 1 A. Since the initial FTS measurements [16] were optimized for the iron spectra, the resolution of each spectrum was chosen to provide roughly 3 to 4 points per full width at half maximum of the iron lines and ranged from 0.08 cm^{-1} in the VUV to 0.03 cm^{-1} in the near UV region. The line widths were dominated by Doppler broadening and thus were proportional to wave number. For neon lines, the full line width at half-maximum was greater than the width of the iron lines by a factor of 1.7 and varied from approximately 0.5 cm^{-1} in the VUV to approximately 0.2 cm^{-1} in the visible region. Between 15 and 20 scans were co-added for each spectrum in the visible region, with 4 to 10 scans being co-added in the UV and the VUV regions. The other experimental details were described in reference [16].

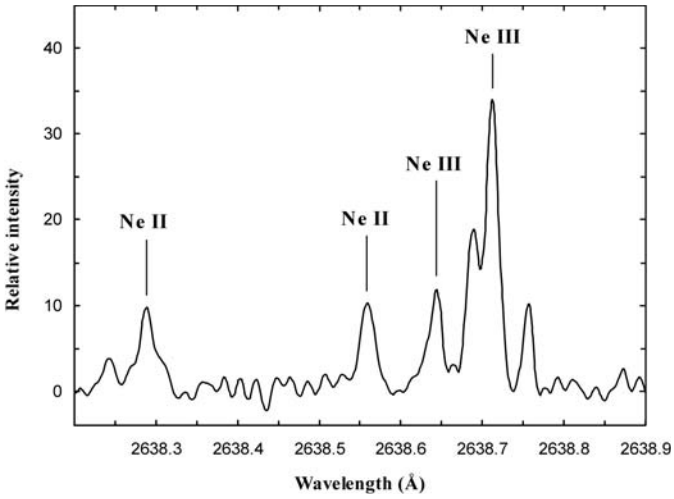

Fig. 1. A portion of a spectrum of an iron-neon hollow cathode lamp. Four scans were taken with 2 to 3 Torr of neon at a current of 350 mA.

A portion of an observed spectrum containing some lines of Ne II and Ne III is presented in Figure 1. The neon lines usually had a noticeable asymmetry caused by the presence of approximately 9% of the ^{22}Ne isotope in the natural neon gas that consists primarily of ^{20}Ne. To verify that the asymmetry of the lines does not significantly affect the derived positions of peaks, we decomposed several isolated line profiles into pairs of peaks. The difference of the wave numbers obtained for the strongest peak in each of the decomposed profiles from the values obtained by fitting the profile with a single peak was always much smaller than the measurement uncertainty.

Apart from the asymmetry, the neon lines could usually be distinguished from the iron lines by their larger width. However, both the larger width and asymmetry can also be caused by blending of two or more lines. Thus, we excluded from our list of Ne III lines those lines identified in the FTS spectra that could possibly be blended with lines of Fe I or Fe II. Such possible blends were identified by existence of an allowed dipole transition between two opposite-parity levels of Fe I or Fe II [17] with a wavelength within the half-width of the measured Ne III line.

The uncertainties of the wave numbers measured by FTS consist of two qualitatively different contributions, the statistical uncertainty $\delta\sigma_{stat}$ and the residual uncertainty $\delta\sigma_r$ which is in turn a combination of the calibration uncertainty (which is dominant) and other systematic errors such as illumination shifts [16]. For iron lines, it was determined in reference [16] that the statistical uncertainty (one standard deviation) can be approximately described by the following formula:

$$\delta\sigma_{stat(\mathrm{Fe})} \approx W/(2S/N), \qquad (1)$$

where W is the line width (full width at half maximum), and S/N is the signal-to-noise ratio of the line. This simplified formula was derived from a more rigorous relation given by Brault [18]:

$$\delta\sigma_{stat} = kW/((S/N)N_w^{1/2}), \quad (2)$$

where N_w is the number of statistically-independent data points per W, and k is a coefficient depending on the type of line profile used in the deconvolution procedure, the recommended value of which is 0.75. The simplified formula (1) takes into account the fact that different scans that were co-added in our spectrograms had different limited wavelength spans and different resolution. The resolution of the scans was varied so that the average number of data points per iron line width was 3 to 4. As it follows from equation (2), in order to account for the increased number of data points per the larger width of the neon lines, the right-hand side of equation (1) should be divided by the square root of the mean ratio of widths of neon and iron lines. Thus, for neon lines equation (1) should be re-written as follows:

$$\delta\sigma_{stat(\mathrm{Ne})} \approx W/(2.6S/N). \quad (3)$$

In the present work we used equation (3) to estimate $\delta\sigma_{stat}$ for neon lines. The value of $\delta\sigma_{stat}$ varied between 0.0005 cm^{-1} for the strongest Ne III lines and 0.06 cm^{-1} for the weakest lines.

The residual uncertainty $\delta\sigma_r$, according to reference [16], was approximately $5 \times 10^{-8}\sigma$ for the visible region and $1 \times 10^{-7}\sigma$ for the VUV and UV regions. The Fe measurements in reference [16] were calibrated with respect to 26 Ar II lines between 4300 Å and 5160 Å. The wave numbers for these lines were taken from Norlén [19], who used Fabry-Perot interferometry to measure them with respect to standard lines in ^{86}Kr. The Ar II lines used have since been remeasured by Whaling et al. [20] using Fourier transform spectroscopy with molecular CO lines as wave number standards. The wave numbers of Whaling et al. are systematically higher than those of Norlén by 6.7 parts in 10^8. Since Whaling's wavenumbers are of higher accuracy than those of Norlén, we have increased the wave numbers of Ne III lines measured in the Fe/Ne spectra by a factor of $6.7 \times 10^{-8}\sigma$ to bring them on the scale of Whaling et al. [20]. The total uncertainty of the measured wave numbers ranged from 0.004 cm^{-1} for the strongest lines to 0.06 cm^{-1} for the weakest lines with signal-to-noise ratio 3 to 4.

3 Analysis of possible Stark shifts

Stark shifts and pressure shifts might affect the wave numbers of the lines in our spectra and in the other studies used in this compilation. To detect these shifts, we have compared the wave numbers in our Fe/Ne spectra measured with different pressures of neon and also with the grating measurements of Sansonetti et al. [10]. The results of this comparison are presented in Figure 2. Panel (a) shows the shifts between two of our FT spectra: one taken at medium neon pressures (2 Torr to 3 Torr), and the other taken at roughly 0.5 Torr neon pressure. Panel (b) shows the shifts between the lines listed in the Pt/Ne atlas [10] and our FT spectrum taken at medium pressure. The lines given in the Pt/Ne atlas [10] were measured using two different lamps, one with roughly 5 Torr of neon and the other with roughly 2 Torr of neon. The line shifts are plotted in Figure 2 vs. the energy of the upper level of the transition. If the Stark shifts were present in the light sources, they would be largest for the lines with the highest upper energy and angular momentum. This would result in increased scatter for higher excitation energies. Figure 2 shows that there is no such trend in our spectra. Furthermore, if Stark shifts were present, they would be accompanied by a noticeable broadening of lines originating from levels with high angular momentum. We observed only a few weak lines originating from the $4f$, $5f$, $7f$, and $7g$ shells. Among these lines, only the $2p^3(^4\mathrm{S}^\circ)3d\ ^3\mathrm{D}^\circ_3$–$2p^3(^4\mathrm{S}^\circ)4f\ ^3\mathrm{F}_4$ line at 1946.0024 Å had signal to noise ratio greater than 4. This line had approximately the same relative width as the rest of the neon lines. The other lines originating from the nf and ng shells were either too weak or blended.

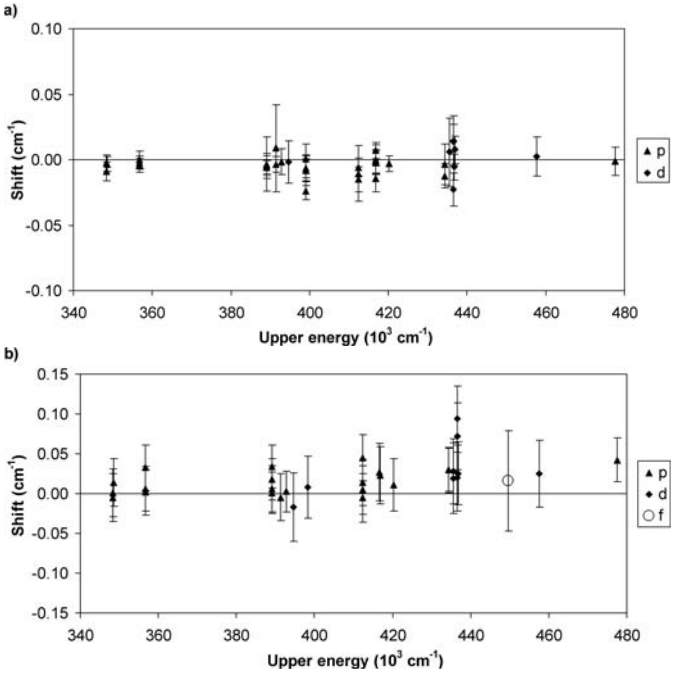

Fig. 2. Wave-number differences between Ne III lines measured in different spectra. (a) Shifts between lines measured in the present work at medium (2 Torr to 3 Torr) and low (0.5 Torr) pressures of neon in the Fe/Ne hollow-cathode discharge; (b) shifts between the grating spectrum of a Pt/Ne hollow cathode [10] and our FT spectrum of a Fe/Ne hollow cathode discharge operated at medium pressure (2 Torr to 3 Torr). The legends describe the orbital momentum of the outer electron for the upper energy level of a transition: (▲) p shell, (♦) d shell, and (○) f shell.

Although there was no direct measurement of Stark shifts in the work of Persson et al. [9], in an earlier work [7] Persson mentioned that even the highest observed members of the $4f-ng$ series showed no noticeable broadening in the Ne II spectra obtained with a hollow cathode lamp operated at very low pressures (0.05 Torr to 0.08 Torr). Since Persson et al. [9] used the same hollow-cathode light source as Persson [7], there should be no noticeable Ne III line broadening in reference [9]. This is also supported by the fact that the stated uncertainty of the wavelengths is approximately the same in reference [9] as in reference [7], implying that the line widths were similar for Ne II and Ne III.

Thus, we conclude that there is no evidence that any of the spectra used in this work exhibit Stark shifts exceeding the wavelength-measurement uncertainty.

4 Optimization procedure

In order to obtain the optimized energy levels, one needs to know the experimental uncertainties of each measured spectral line. Wherever possible, we used estimates of these uncertainties given by the authors of the papers in which the lines were measured. In some cases, the authors gave uncertainties individually for each line [5,12] or indicated an unambiguous procedure describing how to derive them from their tables [10]. In reference [10], the wavelength uncertainty was 0.002 Å for the wavelengths given with three digits after the decimal point (those were measured on photographic plates) and 0.01 Å to 0.02 Å for the wavelengths given with two digits after the decimal point (measured using a scanning photomultiplier in a photon-counting mode).

In other papers, e.g. reference [9], only some general notes were given on the experimental uncertainties for intense separated lines with symmetrical profiles. Unfortunately, Persson et al. [9] did not indicate exactly which of the lines listed by them were measured in the hollow-cathode spectrum and which in the theta-pinch. The corresponding uncertainties, according to the authors' note, should differ by an order of magnitude (a few thousandths and few hundredths of an angstrom). Nevertheless, all wavelengths were given in reference [9] with the same number of digits after the decimal point. We estimated the uncertainties of the lines from reference [9] based on the analysis of deviations of observed wavelengths from those derived from the level values listed in the same paper. As it appears from this analysis, the most intense lines from reference [9] have a standard deviation of 0.003 Å throughout the entire spectral region 1250 Å to 4500 Å where they are located, provided they are not blended or affected by other lines. These lines have intensities greater than 15 on the scale used in reference [9] (300 on our scale; see below), with the exception of the line at 2639.13 Å with intensity 20 (400 on our scale) that deviated by 0.008 Å from its calculated position. The observed intensity and wavelength of this line were probably affected by a stronger neighboring line at 2639.1674 Å. Our calculations with Cowan's codes showed that the intensity of the 2639.13 Å line should be equal to approximately 1/15th of the 2639.1674 Å line, while reference [9] reports the intensity ratio of 2:3. Obviously, the 2639.13 Å line should be a small hump on the shoulder of the 2639.1674 Å line. Thus, we assumed a larger uncertainty of 0.03 Å for this line.

We divided the line list of reference [9] into several categories based on their character (as specified in Tabs. II, III, and IV of Ref. [9]) and wavelength region. The average deviations of the lines with no special character (blended, affected, etc.) having intensities less than 15 on the scale of reference [9] were distinctly different in the wavelength regions 300 Å to 1490 Å (0.006 Å), 1491 Å to 2738 Å (0.009 Å), and 2738 Å to 6900 Å (0.02 Å). The lines denoted as wide, unresolved, blended, affected, etc. displayed an average deviation of 0.05 Å regardless of their intensity. Although all wavelengths were given in reference [9] with three digits after the decimal point, we accepted the average deviations mentioned above as the measurement uncertainties of these lines and rounded the wavelength values accordingly.

Livingston et al. [13] stated that their experimental absolute wavelength uncertainties do not exceed 0.l Å. This is consistent with the line widths of approximately 0.2 Å. We adopted the uncertainty of 0.1 Å for isolated lines but doubled this value for the lines marked in reference [13] as blended, as well as for multiply classified lines.

To find the new values of energy levels based on the whole list of observed wavelengths, we used a new computer program, "LOPT", for optimization of energy level values. This program is described in the Appendix.

To obtain a correct optimization for blended lines, one needs to use proper weights for components of the blend. For example, the center of gravity of a line that is a blend of two transitions with different intensities is not located equidistant to the two components; it shifts towards the component with greater intensity. Thus, in order to correctly represent the influence of the blends on the positions of their upper and lower levels, one needs to know the relative intensities of the component transitions. Although this information is rarely available from experiments, it can be obtained by theoretical calculations. In the present work, we calculated the relative intensities of the lines using Cowan's codes [22] with fitted Slater parameters, assuming the Boltzmann distribution of level populations. The parametric fitting procedure is described below in Section 7. Although the real level population in a hollow-cathode plasma is rather far from the Boltzmann distribution, the errors introduced in the resulting levels by blended lines are usually small because of the low weight ascribed to blended lines. In addition, relative intensities of the lines originating from the same upper level do not depend on the population distribution. In the Ne III spectrum, most of the unresolved blends belong to this category.

5 Energy levels

The list of energy levels obtained as a result of the optimization procedure is presented in Table 1.

Table 1. Energy levels of Ne III.

Configuration	Term[a]	J	Energy[b] (cm^{-1})		Uncert.[c] (cm^{-1})	Leading percentages[d]			
$2s^2 2p^4$	^{3}P	2	0.000		*fixed*	100%			
		1	642.876		0.013	100%			
		0	920.550		0.013	100%			
$2s^2 2p^4$	^{1}D	2	25840.72		0.2	100%			
$2s^2 2p^4$	^{1}S	0	55752.7		0.9	98%			
$2s2p^5$	^{3}P°	2	*204290.0*		1.1	99%			
		1	*204872.6*		1.1	99%			
		0	*205194*		2	99%			
$2s2p^5$	^{1}P°	1	*289478.6*		1.0	98%			
$2s^2 2p^3(^4$S°$)3s$	^{5}S°	2	*309881.041*	$+ x$	2	100%			
$2s^2 2p^3(^4$S°$)3s$	^{3}S°	1	*319431.261*		0.9	100%			
$2s^2 2p^3(^4$S°$)3p$	^{5}P	1	348395.524	$+ x$	0.004	99%			
		2	348426.628	$+ x$	0.004	99%			
		3	348479.578	$+ x$	0.004	99%			
$2s^2 2p^3(^2$D°$)3s$	^{3}D°	3	*353133.605*		0.05	100%			
		2	*353163.013*		0.05	100%			
		1	*353183.152*		0.05	100%			
$2s^2 2p^3(^4$S°$)3p$	^{3}P	1	356751.837		0.004	95%			
		0	356761.864		0.004	95%			
		2	356762.797		0.004	95%			
$2s^2 2p^3(^2$D°$)3s$	^{1}D°	2	*357928.972*		0.06	100%			
$2s^2 2p^3(^2$P°$)3s$	^{3}P°	1	*374489.507*		0.05	98%			
		0	*374490.160*		0.05	98%			
		2	*374496.068*		0.05	98%			
$2s^2 2p^3(^2$P°$)3s$	^{1}P°	1	*379826.356*		0.06	98%			
$2s^2 2p^3(^2$D°$)3p$	^{1}P	1	387962.12		0.06	86%	7%	$(^2$P°$)3p$	^{1}P
$2s^2 2p^3(^2$D°$)3p$	^{3}D	1	389044.544		0.05	91%	6%	$(^2$D°$)3p$	^{1}P
		2	389055.543		0.05	97%			
		3	389124.913		0.05	97%			
$2s^2 2p^3(^2$D°$)3p$	^{3}F	2	391400.239		0.05	100%			
		3	391415.686		0.05	99%			
		4	391436.251		0.05	100%			
$2s^2 2p^3(^2$D°$)3p$	^{1}F	3	392801.818		0.06	100%			
$2s^2 2p^3(^4$S°$)3d$	^{5}D°	4	*394681.481*	$+ x$	0.010	100%			
		3	*394684.08*	$+ x$	0.02	100%			
		2	*394687.67*	$+ x$	0.03	100%			
		1	*394690.72*	$+ x$	0.04	100%			
		0	*394692.40*	$+ x$	0.08	100%			

Table 1. *Continued.*

Configuration	Term[a]	J	Energy[b] (cm^{-1})		Uncert.[c] (cm^{-1})	Leading percentages[d]			
$2s^2 2p^3(^4S^\circ)3d$	$^3D^\circ$	1	*398178.14*		0.04	99%			
		2	*398182.766*		0.03	99%			
		3	*398195.511*		0.02	99%			
$2s^2 2p^3(^2D^\circ)3p$	^3P	2	398972.658		0.05	92%			
		1	399068.682		0.05	93%			
		0	399111.356		0.05	93%			
$2s^2 2p^3(^2D^\circ)3p$	^1D	2	406332.411		0.05	90%	8%	$(^2P^\circ)3p$	^1D
$2s^2 2p^3(^2P^\circ)3p$	^3S	1	409873.45		0.06	98%			
$2s^2 2p^3(^2P^\circ)3p$	^3D	3	412348.045		0.06	97%			
		2	412375.508		0.05	96%			
		1	412376.48		0.05	96%			
$2s^2 2p^3(^2P^\circ)3p$	^1P	1	414229.20		0.06	90%	8%	$(^2D^\circ)3p$	^1P
$2s^2 2p^3(^2P^\circ)3p$	^3P	0	416723.444		0.05	95%			
		1	416753.058		0.05	94%			
		2	416798.087		0.06	94%			
$2s^2 2p^3(^4S^\circ)4s$	$^5S^\circ$	2	*416914.74*	$+ x$	0.07	100%			
$2s^2 2p^3(^4S^\circ)4s$	$^3S^\circ$	1	*419827.35*		0.04	100%			
$2s^2 2p^3(^2P^\circ)3p$	^1D	2	420244.544		0.06	90%	7%	$(^2D^\circ)3p$	^1D
$2s^2 2p^3(^4S^\circ)4p$	^5P	1	430067.99	$+ x$	0.06	100%			
		2	430078.62	$+ x$	0.04	100%			
		3	430095.71	$+ x$	0.04	100%			
$2s^2 2p^3(^2P^\circ)3p$	^1S	0	433011.918		0.06	95%			
$2s^2 2p^3(^4S^\circ)4p$	^3P	2	434325.760		0.02	95%			
		1	434343.564		0.03	95%			
		0	434359.09		0.14	95%			
$2s^2 2p^3(^2D^\circ)3d$	$^3F^\circ$	2	*435515.599*		0.05	99%			
		3	*435555.356*		0.05	99%			
		4	*435608.467*		0.06	98%			
$2s^2 2p^3(^2D^\circ)3d$	$^1S^\circ$	0	*435583.09*		0.09	100%			
$2s^2 2p^3(^2D^\circ)3d$	$^3G^\circ$	5	*436547.744*		0.05	100%			
		4	*436574.426*		0.05	99%			
		3	*436597.709*		0.05	99%			
$2s^2 2p^3(^2D^\circ)3d$	$^1G^\circ$	4	*436771.674*		0.06	100%			
$2s^2 2p^3(^2D^\circ)3d$	$^3D^\circ$	3	*436832.07*		0.06	98%			
		2	*436901.63*		0.05	98%			
		1	*436947.05*		0.06	98%			
$2s^2 2p^3(^2D^\circ)3d$	$^1P^\circ$	1	*439044.19*		0.06	97%			

Table 1. *Continued.*

Configuration	Term[a]	J	Energy[b] (cm^{-1})		Uncert.[c] (cm^{-1})	Leading percentages[d]			
$2s^2 2p^3(^2D^\circ)3d$	$^3P^\circ$	2	*439573.05*		0.07	99%			
		1	*439694.78*		0.07	99%			
		0	*439747.80*		0.10	99%			
$2s^2 2p^3(^2D^\circ)3d$	$^1D^\circ$	2	*439748.13*		0.06	97%			
$2s^2 2p^3(^2D^\circ)3d$	$^3S^\circ$	1	*440051.58*		0.07	100%			
$2s^2 2p^3(^2D^\circ)3d$	$^1F^\circ$	3	*440887.276*		0.06	99%			
$2s^2 2p^3(^4S^\circ)4d$	$^5D^\circ$	4	*446375.1*	$+ x$	0.3	100%			
		2	*446375.17*	$+ x$	0.2	100%			
		3	*446375.73*	$+ x$	0.2	100%			
$2s^2 2p^3(^4S^\circ)4d$	$^3D^\circ$	1	*448223.06*		0.12	98%			
		2	*448233.86*		0.11	98%			
		3	*448251.88*		0.08	98%			
$2s^2 2p^3(^4S^\circ)4f$	^5F	5	449552.15	$+ x$	0.10	100%			
		4	449552.39	$+ x$	0.11	100%			
		3	449552.77	$+ x$	0.11	100%			
		1	449552.9	$+ x$	0.3	100%			
		2	449553.0	$+ x$	0.3	100%			
$2s^2 2p^3(^4S^\circ)4f$	^3F	4	449582.924		0.04	100%			
		3	449583.48		0.12	100%			
		2	449584.03		0.10	100%			
$2s^2 2p^3(^4S^\circ)5s$	$^5S^\circ$	2	*456498.3*	$+ x$	0.09	100%			
$2s^2 2p^3(^2P^\circ)3d$	$^3F^\circ$	4	*457596.833*		0.05	98%			
		3	*457666.99*		0.07	97%			
		2	*457713.80*		0.06	96%			
$2s^2 2p^3(^4S^\circ)5s$	$^3S^\circ$	1	*457782.4*		0.2	100%			
$2s^2 2p^3(^2D^\circ)4s$	$^3D^\circ$	2	*457966.99*		0.09	57%	25%	$(^2P^\circ)3d$	$^3D^\circ$
		3	*457991.30*		0.10	69%	30%	$(^2P^\circ)3d$	$^3D^\circ$
		1	*458001.59*		0.10	70%	29%	$(^2P^\circ)3d$	$^3D^\circ$
$2s^2 2p^3(^2P^\circ)3d$	$^1D^\circ$	2	*458095.49*		0.06	58%	13%	$(^2D^\circ)4s$	$^3D^\circ$
$2s^2 2p^3(^2P^\circ)3d$	$^3P^\circ$	0	*458285.80*		0.13	98%			
		1	*458335.50*		0.11	98%			
		2	*458442.48*		0.09	90%	6%	$(^2P^\circ)3d$	$^1D^\circ$
$2s^2 2p^3(^2P^\circ)3d$	$^3D^\circ$	1	*460114.91*		0.09	68%	29%	$(^2D^\circ)4s$	$^3D^\circ$
		2	*460126.70*		0.08	68%	30%	$(^2D^\circ)4s$	$^3D^\circ$
		3	*460138.75*		0.08	67%	30%	$(^2D^\circ)4s$	$^3D^\circ$
$2s^2 2p^3(^2P^\circ)3d$	$^1F^\circ$	3	*460120.25*		0.07	97%			
$2s^2 2p^3(^2D^\circ)4s$	$^1D^\circ$	2	*460688.20*		0.06	82%	17%	$(^2P^\circ)3d$	$^1D^\circ$
$2s^2 2p^3(^4S^\circ)5p$	^5P	1	462473.29	$+ x$	0.15	100%			
		2	462476.73	$+ x$	0.14	100%			
		3	462482.8	$+ x$	0.2	100%			

Table 1. *Continued.*

Configuration	Term[a]	J	Energy[b] (cm^{-1})		Uncert.[c] (cm^{-1})	Leading percentages[d]			
$2s^22p^3(^2P^\circ)3d$	$^1P^\circ$	1	*462932.64*		0.12	97%			
$2s^22p^3(^4S^\circ)5p$	^3P	2	463856.46		0.08	95%			
		1	463862.3		0.2	95%			
$2s^22p^3(^4S^\circ)5d$	$^5D^\circ$	4	*470197.0*	$+ x$	0.3	100%			
		3	*470198.9*	$+ x$	0.9	100%			
		2	*470199.5*	$+ x$	0.9	100%			
$2s^22p^3(^4S^\circ)5d$	$^3D^\circ$	2	*471181.0*		0.6	99%			
		3	*471181.0*		0.4	99%			
$2s^22p^3(^2D^\circ)4p$	^3D	1	471233.53		0.06	86%	13%	$(^2D^\circ)4p$	^1P
		2	471273.90		0.06	99%			
		3	471283.81		0.05	99%			
$2s^22p^3(^2D^\circ)4p$	^1P	1	471385.12		0.11	86%	13%	$(^2D^\circ)4p$	^3D
$2s^22p^3(^4S^\circ)5f$	^5F		471871.5	$+ x$	0.4	100%			
$2s^22p^3(^4S^\circ)5f$	^3F	4	471889.71		0.09	98%			
		3	471890.19		0.11	98%			
		2	471890.24		0.14	99%			
$2s^22p^3(^4S^\circ)5g$	$^5G^\circ$		*472004.1*	$+ x$	0.4	100%			
$2s^22p^3(^4S^\circ)5g$	$^3G^\circ$	5	*472004.38*		0.05	100%			
		4	*472004.44*		0.12	100%			
		3	*472004.52*		0.11	100%			
$2s^22p^3(^2D^\circ)4p$	^3F	4	472013.12		0.06	98%			
		3	472020.08		0.06	98%			
		2	472027.94		0.05	98%			
$2s^22p^3(^2D^\circ)4p$	^1F	3	472473.64		0.06	100%			
$2s^22p^3(^2D^\circ)4p$	^3P	2	473863.42		0.09	93%			
		1	473932.50		0.12	94%			
		0	473963.62		0.12	94%			
$2s^22p^3(^4S^\circ)6s$	$^5S^\circ$	2	*475542.98*	$+ x$	0.13	100%			
$2s^22p^3(^2D^\circ)4p$	^1D	2	477534.680		0.06	96%			
$2p^6$	^1S	0	478826		2	95%			
$2s^22p^3(^2P^\circ)4s$	$^3P^\circ$	1	*479827.5*		0.2	97%			
		2	*479831.5*		0.2	97%			
		0	*479836.38*		0.11	97%			
$2s^22p^3(^2P^\circ)4s$	$^1P^\circ$	1	*481288.0*		0.2	96%			
$2s^22p^3(^4S^\circ)6d$	$^3D^\circ$		*483600*		200	99%			

Table 1. *Continued.*

Configuration	Term[a]	J	Energy[b] (cm^{-1})		Uncert.[c] (cm^{-1})	Leading percentages[d]				
$2s^2 2p^3(^4S^\circ)6f$	^5F		484001.3	$+ x$	0.7	100%				
$2s^2 2p^3(^4S^\circ)6f$	^3F	3	484018.8		0.4	100%				
		4	484019.1		0.4	100%				
		2	484019.5		0.3	100%				
$2s^2 2p^3(^4S^\circ)6g$	$^5G^\circ$		*484083.8*	$+ x$	0.5	100%				
$2s^2 2p^3(^4S^\circ)6g$	$^3G^\circ$	3	*484084.0*		0.5	100%				
		4	*484084.0*		0.5	100%				
		5	*484084.0*		0.5	100%				
$2s^2 2p^3(^4S^\circ)7s$	$^5S^\circ$	2	*486165.7*	$+ x$	0.3	100%				
$2s^2 2p^3(^2D^\circ)4d$	$^3F^\circ$	3	*487624.9*		0.13	99%				
		4	*487633.1*		0.3	98%				
$2s^2 2p^3(^2D^\circ)4d$	$^3G^\circ$	5	*487908.04*		0.08	100%				
		4	*487930.17*		0.08	98%				
		3	*487953.47*		0.07	99%				
$2s^2 2p^3(^2D^\circ)4d$	$^1G^\circ$	4	*488046.23*		0.13	99%				
$2s^2 2p^3(^2D^\circ)4d$	$^3D^\circ$		*488100*		600	96%				
$2s^2 2p^3(^2D^\circ)4d$	$^3P^\circ$		*489000*		500	98%				
$2s^2 2p^3(^2D^\circ)4d$	$^3S^\circ$	1	*489000*	?	800	99%				
$2s^2 2p^3(^2D^\circ)4d$	$^1P^\circ$	1	*489200*		900	97%				
$2s^2 2p^3(^2D^\circ)4d$	$^1D^\circ$	2	*489200*		500	99%				
$2s^2 2p^3(^2D^\circ)4d$	$^1F^\circ$	3	*489900*		400	99%				
$2s^2 2p^3(^4S^\circ)7d$	$^3D^\circ$		*490000*	?	500	97%				
$2s^2 2p^3(^2D^\circ)4f$	^3G	5	490789.83		0.10	87%		8%	$(^2D^\circ)4f$	^3H
		4	490790.7		0.2	45%	^3F	44%	$(^2D^\circ)4f$	^3G
		3	490794.29		0.14	41%		30%	$(^2D^\circ)4f$	^3D
$2s^2 2p^3(^2D^\circ)4f$	^3D	2	490798.4		0.15	37%	^1D	36%	$(^2D^\circ)4f$	^3D
		3	490800.17		0.11	54%		35%	$(^2D^\circ)4f$	^3G
		1	490888.1		1.3	95%				
$2s^2 2p^3(^2D^\circ)4f$	^3F	4	490800.19		0.11	51%		47%	$(^2D^\circ)4f$	^3G
		3	490815.12		0.10	71%		17%	$(^2D^\circ)4f$	^3G
		2	490837.45		0.11	68%		28%	$(^2D^\circ)4f$	^3D
$2s^2 2p^3(^2D^\circ)4f$	^1P	1	490811.32		0.14	90%		10%	$(^2D^\circ)4f$	^3P
$2s^2 2p^3(^2D^\circ)4f$	^1D	2	490819.04		0.13	59%		36%	$(^2D^\circ)4f$	^3D
$2s^2 2p^3(^2D^\circ)4f$	^3H	5	490832.60		0.09	53%		34%	$(^2D^\circ)4f$	^1H
		6	490833.55		0.11	100%				
		4	490885.32		0.11	95%				

Table 1. *Continued.*

Configuration	Term[a]	J	Energy[b] (cm^{-1})		Uncert.[c] (cm^{-1})	Leading percentages[d]			
$2s^2 2p^3(^2D^\circ)4f$	^1G	4	490833.93		0.10	84%	9%	$(^2D^\circ)4f$	^3G
$2s^2 2p^3(^2D^\circ)4f$	^3P	1	490835.4		0.2	87%	9%	$(^2D^\circ)4f$	^1P
		0	490840.7		0.2	100%			
		2	490894.98		0.14	99%			
$2s^2 2p^3(^2D^\circ)4f$	^1F	3	490853.30		0.10	88%	6%	$(^2D^\circ)4f$	^3G
$2s^2 2p^3(^2D^\circ)4f$	^1H	5	490882.41		0.09	61%	39%	$(^2D^\circ)4f$	^3H
$2s^2 2p^3(^4S^\circ)7f$	^5F		491313.3	$+ x$	0.3	100%			
$2s^2 2p^3(^4S^\circ)7f$	^3F	4	491326.9		0.5	100%			
$2s^2 2p^3(^4S^\circ)7g$	$^5G^\circ$		*491369.4*	$+ x$	0.6	100%			
$2s^2 2p^3(^4S^\circ)7g$	$^3G^\circ$	3	*491369.6*		0.5	100%			
		4	*491369.6*		0.5	100%			
		5	*491369.6*		0.5	100%			
$2s^2 2p^3(^2P^\circ)4p$	^3S	1	492224.55		0.2	98%			
$2s^2 2p^3(^4S^\circ)8s$	$^5S^\circ$	2	*492692.1*	$+ x$	0.4	100%			
$2s^2 2p^3(^2P^\circ)4p$	^3D	1	492947.4		0.2	96%			
		3	492947.9		0.2	98%			
		2	492954.3		0.14	98%			
$2s^2 2p^3(^2P^\circ)4p$	^1P	1	493158.9		0.2	94%			
$2s^2 2p^3(^2P^\circ)4p$	^3P	0	493572.1		0.3	94%			
		1	493596.0		0.3	93%			
		2	493603.4		0.3	94%			
$2s^2 2p^3(^2P^\circ)4p$	^1D	2	495312.2		0.3	96%			
$2s^2 2p^3(^4S^\circ)8f$	^5F		496060.0	$+ x$	0.4	100%			
$2s^2 2p^3(^2D^\circ)5s$	$^3D^\circ$	3	*497994.44*		0.09	100%			
		2	*498020.88*		0.10	100%			
		1	*498039.74*		0.12	100%			
$2s^2 2p^3(^2D^\circ)5s$	$^1D^\circ$	2	*498658.714*		0.07	100%			
$2s^2 2p^3(^2D^\circ)5p$	^3F	4	504103.2		0.2	100%			
		3	504115.9		0.2	99%			
		2	504131.3		0.2	100%			
$2s^2 2p^3(^2P^\circ)4d$	$^1F^\circ$	3	*510300*		200	97%			
$2s^2 2p^3(^2P^\circ)4d$	$^1P^\circ$	1	*511100*	?	400	57%	42%	$(^2D^\circ)5d$	$^1P^\circ$
$2s^2 2p^3(^2P^\circ)4f$	^3D	1	511901.1		1.5	95%			
		2	511907.92		0.11	87%	7%	$(^2P^\circ)4f$	^1D
		3	511933.8		0.3	84%	6%	$(^2P^\circ)4f$	^3F

Table 1. *Continued.*

Configuration	Term[a]	J	Energy[b] (cm^{-1})		Uncert.[c] (cm^{-1})	Leading percentages[d]			
$2s^22p^3(^2\mathrm{P}^\circ)4f$	^{1}D	2	511953.1		0.2	67%		26%	$(^2\mathrm{P}^\circ)4f$ ^{3}F
$2s^22p^3(^2\mathrm{P}^\circ)4f$	^{3}G	5	511960.0		0.3	96%			
		4	511966.3		0.3	80%		16%	$(^2\mathrm{P}^\circ)4f$ ^{3}F
		3	511974.6		0.4	74%		14%	$(^2\mathrm{P}^\circ)4f$ ^{1}F
$2s^22p^3(^2\mathrm{P}^\circ)4f$	^{1}G	4	511996.8		1.1	69%		20%	$(^2\mathrm{P}^\circ)4f$ ^{3}F
$2s^22p^3(^2\mathrm{P}^\circ)4f$	^{1}F	3	512036.7		0.14	46%	^{3}F	40%	$(^2\mathrm{P}^\circ)4f$ ^{1}F
$2s^22p^3(^2\mathrm{P}^\circ)4f$	^{3}F	2	512041.8		0.3	71%		21%	$(^2\mathrm{P}^\circ)4f$ ^{1}D
		3	512058.43		0.14	38%		37%	$(^2\mathrm{P}^\circ)4f$ ^{1}F
		4	512063.2		0.2	62%		26%	$(^2\mathrm{P}^\circ)4f$ ^{1}G
$2s^22p^3(^2\mathrm{D}^\circ)5d$	^{1}F°	3	*512900*	?	600	98%			
$2s^22p^3(^2\mathrm{D}^\circ)5f$	^{3}H	5	513139.8		0.3	59%		41%	$(^2\mathrm{D}^\circ)5f$ ^{1}H
		6	513141.3		0.2	100%			
		4	513159.7		0.2	100%			
$2s^22p^3(^2\mathrm{D}^\circ)5f$	^{3}G	5	513154.05		0.14	97%			
		4	513195.13		0.08	63%		30%	$(^2\mathrm{D}^\circ)5f$ ^{3}F
$2s^22p^3(^2\mathrm{D}^\circ)5f$	^{1}H	5	513197.2		0.2	59%		41%	$(^2\mathrm{D}^\circ)5f$ ^{3}H
$2s^22p^3(^2\mathrm{D}^\circ)5f$	^{1}G	4	513210.29		0.13	86%		10%	$(^2\mathrm{D}^\circ)5f$ ^{3}G
$2s^22p^3(^2\mathrm{D}^\circ)5g$	^{3}I°	5	*513245.5*		0.2	91%		5%	$(^2\mathrm{D}^\circ)5g$ ^{1}H°
		6	*513245.5*		0.2	49%		42%	$(^2\mathrm{D}^\circ)5g$ ^{1}I°
		7	*513245.5*		0.2	100%			
$2s^22p^3(^2\mathrm{D}^\circ)6g$	^{3}I°	5	*525323.9*		0.6	89%		6%	$(^2\mathrm{D}^\circ)6g$ ^{1}H°
		6	*525323.9*		0.6	48%		41%	$(^2\mathrm{D}^\circ)6g$ ^{1}I°
		7	*525323.9*		0.6	100%			
$2s^22p^3(^2\mathrm{P}^\circ)5d$	^{1}P°	1	*534500*	?	500	96%			

[a]Term labels assigned to levels having a highly mixed composition are somewhat arbitrary. See discussion in the text.
[b]The symbols after the energy have the following meaning: $+x$ – position of the quintet level system relative to the singlet and triplet levels was fixed based on the very small calculated separation between the ^{5}G° and ^{3}G° terms of the $2s^22p^3(^4\mathrm{S}^\circ)ng$ configurations (see text). The value of x should not exceed 2 cm^{-1}; ? – identification of lines determining this level is uncertain.
[c] Uncertainties of the levels with energies below 320000 cm^{-1} are given relative to the ground state. Uncertainties of the higher-energy singlet and triplet levels are given relative to the $2s^22p^3(^4\mathrm{S}^\circ)3s^3\mathrm{S}^\circ_1$ level, and uncertainties of the quintet levels are given relative to the $2s^22p^3(^4\mathrm{S}^\circ)3s^5\mathrm{S}^\circ_2$ level.
[d]Percentage compositions were calculated by parametric fitting calculations using Cowan's codes [22] (see text).

The levels of the Ne III $2s^22p^4$ ground configuration given in Table 1 are more accurate than in reference [9], as they were optimized with the use of additional precisely measured lines. They are in good agreement with values given by Persson [7], although their difference from the values given in reference [9] is in the range –1.0 cm^{-1} to +5.2 cm^{-1}. The uncertainty of the $2p^4\ ^1\mathrm{D}_2$ level is less than 0.2 cm^{-1} relative to the ground state; the levels $^3\mathrm{P}_1$ and $^3\mathrm{P}_0$ are determined with an uncertainty of 0.002 cm^{-1} relative to each other and 0.013 cm^{-1} relative to the ground state. A partial Grotrian diagram illustrating the derivation of the $2p^4\ ^1\mathrm{S}_0$ level is presented in Figure 3. The $2p^4\ ^1\mathrm{S}_0$ level is directly connected with the $2p^4\ ^1\mathrm{D}_2$ level by a line at (3342.5±0.3) Å which is blended with an intercombination line of Cl III, as observed in nebular spectra by Bowen [6]. Another, more precise, connection of the $2p^4\ ^1\mathrm{S}_0$ level with the lower levels of the ground configuration is provided by the (427.8521±0.0018) Å line ($2s^22p^4\ ^1\mathrm{S}_0 - 2s2p^5\ ^1\mathrm{P}^\circ_1$) measured by Brosius et al. [12], combined with a direct transition to the $2p^4\ ^1\mathrm{D}_2$ level

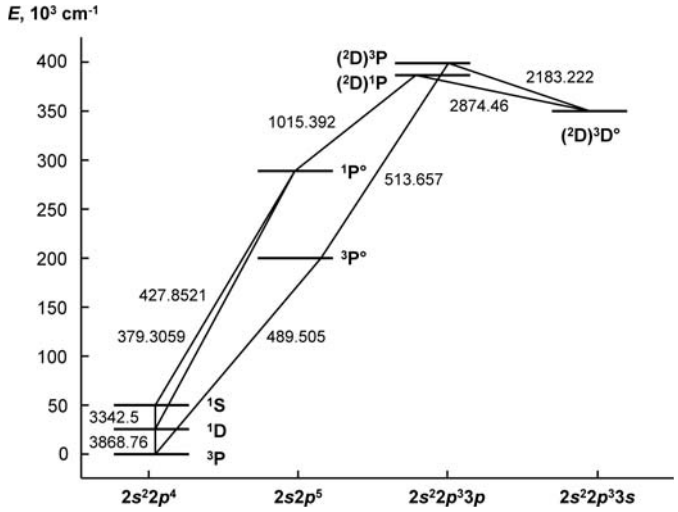

Fig. 3. A partial Grotrian diagram showing the main transitions from which the $2p^4\ ^1S_0$ level is derived. The numbers next to the lines connecting the levels are transition wavelengths in angstroms. The lines responsible for the improvement in accuracy of this level value in the current work are those at 427.8521 ± 0.0018 Å ($2s^22p^4\ ^1S_0 - 2s2p^5\ ^1P_1^\circ$) and 379.3059 ± 0.0013 Å ($2p^4\ ^1D_2 - 2s2p^5\ ^1P_1^\circ$) measured by Brosius et al. [12].

by the 379.3059 ± 0.0013 Å line [12] and several indirect paths, e.g. 1015.392 Å ($3p^1P_1$) + 2874.46 Å ($3s^3D_1^\circ$) + 2183.222 Å ($3p^3P_2$) + 513.657 Å ($2s2p^5\ ^3P_2^\circ$) + 489.505 Å ($2p^4\ ^3P_2$) lines. The weighted average of the energy of the $2p^4\ ^1S_0$ level obtained using these different paths is (55752.7 ± 0.9) cm^{-1}. This should be compared with the value 55747.5 cm^{-1} from Persson et al. [9], who used only their own less precise wavelengths for the 379 Å and 427 Å lines and did not include the 3342.5 Å and 3868.76 Å lines in the level optimization.

It is difficult to adequately represent the uncertainties of the levels, since they differ greatly depending on the choice of the reference level. Uncertainties of most of the excited levels relative to the ground state are defined by the wavelength-measurement uncertainty of the EUV lines connecting the $n = 3$ configurations with the ground configuration $2s^22p^4$ and the first excited configuration $2s2p^5$. This uncertainty is about 0.9 cm^{-1}, which is only slightly less than the uncertainty stated in reference [9]. Nevertheless, we consider our level values to be more accurate because of the improved accuracy of the levels of the ground configuration and the increased number of precise connections to the ground configuration provided by the measurements of Brosius et al. [12]. The average shift of the excited levels relative to the values from reference [9] is about +1.7 cm^{-1}. The excited levels with $n \geq 3$ are determined with much higher accuracy relative to the lowest levels with $n = 3$, because the lines connecting them with each other are located in the wavelength region above 1800 Å. In this wavelength region, precise measurements are easier to make due to availability of accurate wavelength standards and high-precision measurement techniques, such as FTS. The excited level system consists of several "rigid" (i.e. connected by high-precision lines) groups of levels with much weaker (less precise) connections between these groups. This means that, although the relative separations of levels within some groups are as small as 0.003 cm^{-1}, the positions of these level groups relative to each other can be uncertain by few tenths cm^{-1}. Thus, the level uncertainties are given in Table 1 relative to the ground state only for the levels of the $2s^22p^4$ and $2s2p^5$ configurations and for the lowest two $n = 3$ levels, $2s^22p^3\ (^4S^\circ)3s\ ^3S_1^\circ$ and $2s^22p^3\ (^4S^\circ)3s\ ^5S_2^\circ$. Uncertainties of the higher-lying singlet and triplet levels are given relative to the $2s^22p^3\ (^4S^\circ)3s\ ^3S_1^\circ$ level, and for the quintet levels relative to the $2s^22p^3\ (^4S^\circ)3s\ ^5S_2^\circ$ level. To obtain the uncertainty relative to the ground state, the uncertainties of these higher lying levels should be added in quadrature to the uncertainty of the reference level.

Although some of the level values in Table 1 have fewer significant figures than in reference [9], we believe that they are more accurate. We have chosen to round off the levels having relative uncertainties greater than 0.15 cm^{-1} to one decimal place, and those having relative uncertainties between 0.015 cm^{-1} and 0.15 cm^{-1} to two decimal places, in order to better represent their accuracy. Many of the levels given with three figures after the decimal point have uncertainties of the order of 0.05 cm^{-1} relative to the lowest $n = 3$ levels. Nevertheless, the extra digit is necessary in order to reproduce the observed precisely measured wavelengths for some of the lines connecting these levels with each other.

The quintet term system is not connected with the ground state by any observed transition. We introduced a symbol "x" representing an unknown shift of the quintet system relative to the ground state. In reference [9], the relative position of the quintet system was fixed by requiring that the $(^4S^\circ)ng\ ^5G^\circ$ and $^3G^\circ$ terms ($n = 5$ to 7) coincide. We have slightly modified this procedure by introducing small $^5G^\circ - ^3G^\circ$ separations (0.2 to 0.3) cm^{-1}, as indicated by our calculations. According to reference [9], the value of x should not exceed 2 cm^{-1}.

Percentage eigenvector compositions for the levels given in Table 1 were computed in the present work. In most cases they are in good agreement with the results obtained by Persson et al. [9]. If the configuration or parent term of the component is omitted in the column of percentages, it is the same as for the leading component. According to reference [9], the LS designations of the $2s^22p^34f$ levels are based on the observed intensity distribution in the $3d - 4f$ transition array. The $2s^22p^3(^2D^\circ)4f$ level with $J = 2$ at 490798.4 cm^{-1} cannot be labeled appropriately in the LS coupling scheme. We retained the term label ^3D assigned in reference [9] because this character makes one of the most prominent contributions to it, and this term name is not used for any other level. Similar considerations apply to the $4f$ levels at 490790.7 cm^{-1} ($J = 4$), 490794.29 cm^{-1}, 512036.7 cm^{-1}, and 512058.43 cm^{-1} ($J = 3$), as well as the $5g$ and $6g$ levels at 513245.5 cm^{-1} and 525323.9 cm^{-1} ($J = 6$). For these levels, the coupling is too far from pure LS coupling for the labels to have physical meaning.

Since the $(^4S^\circ)ng\ ^5G^\circ$ levels determined in the present study are systematically higher than found in reference [9], the ionization potential determined in reference [9] from this series must be revised. We re-determined the ionization potential using the same procedure of fitting the polarization formula as described in reference [9] using two series, $(^4S^\circ)ng\ ^5G^\circ$ and $(^4S^\circ)ng\ ^3G^\circ$. The results for these two series differ by only 0.4 cm^{-1}. However, since the $(^4S^\circ)ng\ ^3G^\circ$ series does not involve the uncertainty of the $^5G^\circ - ^3G^\circ$ separation, its limit has lower uncertainty. Our final value of the ionization potential derived from the $(^4S^\circ)ng\ ^3G^\circ$ series is (511543.5 ± 2.7) cm^{-1} $(63.4233\ eV \pm 0.0003\ eV)$. To obtain the value in electron volts, we applied the conversion factor 8065.54445(69) cm^{-1}/eV [23].

6 Compiled list of observed lines of Ne III

The list of observed lines of Ne III used in the level optimization is presented in Table 2.

To avoid zero intensity values, intensities of the lines from Persson et al. [9] were converted as $I_{new} = 20I_{old} + 2$. This conversion results in integer numbers comparable with those observed in the EUV range by Livingston et al. [13]. The same conversion was done with intensities from Boyce [3] in order to bring them to the same scale in the region 350 Å to 500 Å. Intensities from von Keussler [2] were multiplied by 10, while those from references [12,14] were divided by 5. For the lines measured in reference [10] and in the present work that were also observed by Persson et al. [9], we used the intensity values from reference [9] converted as described above. After this conversion, the relative intensities of the lines appear to be approximately on the same scale in the entire spectral range.

All lines published by de Bruin [1] were re-measured with higher accuracy by Persson et al. [9]. The authors of reference [9] also revised about 30% of de Bruin's identifications.

As already mentioned above (see Sect. 4), numerous wavelengths from Persson et al. [9] deviate strongly (by 0.03 Å to 0.2 Å) from the Ritz wavelengths derived from the energy levels given in [9]. Nevertheless, they were accepted by the authors of reference [9], implying that the measurement uncertainties were consistent with these large deviations. Both observed and calculated wavelengths have been rounded off according to their estimated uncertainty in Table 2, in order to represent the accuracy better.

In the present compilation, 88 wavelengths from Persson et al. [9] were replaced with those measured more accurately in reference [10] and in the present work. Their uncertainties were discussed above in Section 4. Several lines listed as masked by Persson et al. [9] have been resolved in the spectra observed in reference [10] and in the present work. In particular, three combinations involving the $2s^2 2p^3(^2P^\circ)4s\ ^3P^\circ_0$ level have been resolved that were either masked or blended in Persson's spectrum.

We have replaced several VUV wavelengths measured by Persson et al. [9], von Keussler [2], and Boyce [3] with newer more precise values measured by Brosius et al. [12]. The observed wavelengths of the blended lines reported by Brosius et al. [12] at 267.4884 Å, 283.1745 Å, and 283.6651 Å should be used with caution. The components of these blends have a larger wavelength spread than the measurement uncertainty declared in reference [12]. For such blended lines, the position of the measured line center may depend on the excitation conditions and method of locating the line center.

Thomas and Neupert [24] reported the measurement in a solar spectrum of several VUV lines that they assigned to Ne III. In particular, they interpreted the line they observed at (322.696 ± 0.011) Å as the triplet-quintet intercombination transition $2p^4\ ^3P_2 - 2p^3 3s\ ^5S^\circ_2$. Indeed, the predicted wavelength of this transition derived from our level optimization procedure is (322.7045 ± 0.0011) Å. However, it was convincingly argued by Bhatia et al. [25] that this line, as well as two other lines observed in reference [24], cannot be attributed to Ne III because it is too intense. Recent calculations of Froese Fischer and Tachiev [26] yield a factor-of-three greater transition probability for the $2p^4\ ^3P_2$–$2p^3 3s\ ^5S^\circ_2$ transition than the calculations of Bhatia et al. [25]. However, even with this increased transition probability, the predicted intensity of the $2p^4\ ^3P_2$–$2p^3 3s\ ^5S^\circ_2$ is an order of magnitude lower than observed for the 322.696 Å line.

In the column of uncertainties of the Ritz wavelengths in Table 2, the superscript "*s*" indicates that the Ritz wavelength of the line is suggested as a wavelength standard. There are more than hundred such lines in the region 210 Å to 2000 Å. The lines that we suggest as standards are strong isolated lines that have an estimated uncertainty of the calculated wavelength between 0.0002 Å and 0.0011 Å. There are many more lines with estimated uncertainty in the range 0.0003 Å to 0.002 Å that can be used as reference lines, provided they are well resolved in the observed spectrum.

7 New identifications in the extreme ultraviolet range

In order to evaluate the new identifications for Ne III in the EUV range made recently by Livingston et al. [13] and also the revisions of the Paul and Polster's Ne IV assignments [15] made by Bastin [14], we calculated the transition probabilities of the lines involved. We succeeded in reproducing the parametric fit made by Persson et al. [9], having extended it to all known energy levels. We started from the parameter values given in reference [9], allowing only the average energies to vary. The fit converged with level deviations and percentages close to those obtained in reference [9]. After that, the effective parameters α were allowed to vary. This fitting converged with significantly negative values of α. Since these parameters are supposed to compensate for the unaccounted configuration interactions, it means that the configuration interaction (CI) was overestimated in the initial fitting. Thus, we decreased the values of all CI integrals to an empirically found optimum

Table 2. Observed lines of Ne III (the full version of this table is available in the supplementary *Online Material*).

λ_{obs} (Å)[a]	Obs. unc.(Å)	σ_{obs} (cm^{-1})	Obs. int. and char.[b]	λ_{Ritz} (Å)	Ritz unc.[c](Å)	Transition[d]	A[e] (s^{-1})		Ref. λ[f]	Ref. A[g]
211.5	0.1	472810	2	211.4979	0.0004[s]	$2s^22p^4$ $^1D_2$ – ($^2D^\circ$)$5s$ $^1D^\circ_2$			13	
212.2	0.2	471250	5*bl*	212.2327	0.0005[s]	$2s^22p^4$ $^3P_2$ – ($^4S^\circ$)$5d$ $^3D^\circ_3$			13	
212.5	0.2	470590	9*bl*	212.5226	0.0005[s]	$2s^22p^4$ $^3P_1$ – ($^4S^\circ$)$5d$ $^3D^\circ_2$			13	
217.777	0.010	459190	3*bl*	217.7727	0.0005[s]	$2s^22p^4$ $^3P_0$ – ($^2P^\circ$)$3d$ $^3D^\circ_1$	2.0e+09	C	15	26
218.131	0.010	458440	5*bl*	218.1299	0.0005[s]	$2s^22p^4$ $^3P_2$ – ($^2P^\circ$)$3d$ $^3P^\circ_2$	3.9e+09	B	15	26
218.184	0.010	458330	2*bl*	218.1808	0.0005[s]	$2s^22p^4$ $^3P_2$ – ($^2P^\circ$)$3d$ $^3P^\circ_1$	2.2e+09	B	15	26
223.6	0.1	447230	2	223.5623	0.0005[s]	$2s^22p^4$ $^3P_0$ – ($^4S^\circ$)$4d$ $^3D^\circ_1$			13	
227.5	0.2	439560	12*bl*	227.2461	0.0005[s]	$2s^22p^4$ $^3P_2$ – ($^2D^\circ$)$3d$ $^3S^\circ_1$	8.2e+09	C	13	26
230.0	0.1	434780	2	229.9657	0.0005[s]	$2s^22p^4$ $^1D_2$ – ($^2D^\circ$)$4s$ $^1D^\circ_2$			13	
230.3	0.1	434220	6	230.2664	0.0005[s]	$2s^22p^4$ $^1D_2$ – ($^2P^\circ$)$3d$ $^1F^\circ_3$	1.1e+10	B	13	26
231.3	0.1	432340	4	231.3450	0.0005[s]	$2s^22p^4$ $^1D_2$ – ($^2P^\circ$)$3d$ $^1D^\circ_2$	4.6e+09	C	13	26
238.2	0.1	419820	3	238.1932	0.0006[s]	$2s^22p^4$ $^3P_2$ – ($^4S^\circ$)$4s$ $^3S^\circ_1$			13	
240.9	0.1	415110	18	240.9368	0.0006[s]	$2s^22p^4$ $^1D_2$ – ($^2D^\circ$)$3d$ $^1F^\circ_3$	2.0e+10	C	13	26
241.6	0.1	413910	14	241.5999	0.0006[s]	$2s^22p^4$ $^1D_2$ – ($^2D^\circ$)$3d$ $^1D^\circ_2$	1.5e+10	C	13	26
242.0	0.1	413220	12	242.0115	0.0006[s]	$2s^22p^4$ $^1D_2$ – ($^2D^\circ$)$3d$ $^1P^\circ_1$	1.3e+10	C	13	26
245.6	0.1	407170	7	245.5917	0.0008[s]	$2s^22p^4$ $^1S_0$ – ($^2P^\circ$)$3d$ $^1P^\circ_1$	3.0e+10	D	13	C
251.73	0.02	397260	20	251.7258	0.0006[s]	$2s^22p^4$ $^3P_0$ – ($^4S^\circ$)$3d$ $^3D^\circ_1$	6.3e+09	C	2	26
267.026	0.002	374496	30*bl*	267.0255	0.0007[s]	$2s^22p^4$ $^3P_2$ – ($^2P^\circ$)$3s$ $^3P^\circ_2$	2.8e+09	C	12	26
267.687	0.002	373571	20	267.6882	0.0007[s]	$2s^22p^4$ $^3P_0$ – ($^2P^\circ$)$3s$ $^3P^\circ_1$	1.4e+09	C	12	26
282.495	0.002	353989	20	282.4973	0.0008[s]	$2s^22p^4$ $^1D_2$ – ($^2P^\circ$)$3s$ $^1P^\circ_1$	3.3e+09	C	12	26
283.871	0.005	352273	30	283.8791	0.0008[s]	$2s^22p^4$ $^3P_0$ – ($^2D^\circ$)$3s$ $^3D^\circ_1$	2.0e+09	C	12	26
301.1242	0.0013	332088.9	90	301.1248	0.0009[s]	$2s^22p^4$ $^1D_2$ – ($^2D^\circ$)$3s$ $^1D^\circ_2$	9.2e+09	C	12	26
313.0574	0.0014	319430.2	90	313.0564	0.0009[s]	$2s^22p^4$ $^3P_2$ – ($^4S^\circ$)$3s$ $^3S^\circ_1$	6.1e+09	C	12	26
313.692	0.002	318784	70	313.6877	0.0009[s]	$2s^22p^4$ $^3P_1$ – ($^4S^\circ$)$3s$ $^3S^\circ_1$	3.6e+09	C	12	26
313.964	0.004	318508	30	313.9612	0.0009[s]	$2s^22p^4$ $^3P_0$ – ($^4S^\circ$)$3s$ $^3S^\circ_1$	1.2e+09	C	12	26
831.844	0.006	120214.8	240	831.8452	0.0003[s]	($^4S^\circ$)$3s$ $^5S^\circ_2$ – ($^4S^\circ$)$4p$ $^5P_3$	1.3e+08	D	9	C
831.963	0.006	120197.7	180	831.9635	0.0003[s]	($^4S^\circ$)$3s$ $^5S^\circ_2$ – ($^4S^\circ$)$4p$ $^5P_2$	1.3e+08	D	9	C
832.041	0.006	120186.4	160	832.0371	0.0004[s]	($^4S^\circ$)$3s$ $^5S^\circ_2$ – ($^4S^\circ$)$4p$ $^5P_1$	1.3e+08	D	9	C
841.186	0.006	118879.8	120	841.1878	0.0003[s]	($^2D^\circ$)$3s$ $^3D^\circ_3$ – ($^2D^\circ$)$4p$ $^3F_4$	9.7e+07	D	9	C
841.344	0.006	118857.4	70	841.3467	0.0003[s]	($^2D^\circ$)$3s$ $^3D^\circ_2$ – ($^2D^\circ$)$4p$ $^3F_3$	9.1e+07	D	9	C
841.429	0.006	118845.4	20	841.4336	0.0002[s]	($^2D^\circ$)$3s$ $^3D^\circ_1$ – ($^2D^\circ$)$4p$ $^3F_2$	8.6e+07	D	9	C
846.377	0.006	118150.7	120	846.3802	0.0003[s]	($^2D^\circ$)$3s$ $^3D^\circ_3$ – ($^2D^\circ$)$4p$ $^3D_3$	1.3e+08	D	9	C
846.659	0.006	118111.3	70	846.6620	0.0003[s]	($^2D^\circ$)$3s$ $^3D^\circ_2$ – ($^2D^\circ$)$4p$ $^3D_2$	1.1e+08	D	9	C
847.091	0.006	118051.1	20	847.0960	0.0003[s]	($^2D^\circ$)$3s$ $^3D^\circ_1$ – ($^2D^\circ$)$4p$ $^3D_1$	9.5e+07	D	9	C
870.235	0.006	114911.5	30	870.2288	0.0003[s]	($^4S^\circ$)$3s$ $^3S^\circ_1$ – ($^4S^\circ$)$4p$ $^3P_1$			9	
870.367	0.006	114894.1	50	870.3637	0.0002[s]	($^4S^\circ$)$3s$ $^3S^\circ_1$ – ($^4S^\circ$)$4p$ $^3P_2$			9	
873.023	0.006	114544.5	90	873.0219	0.0003[s]	($^2D^\circ$)$3s$ $^1D^\circ_2$ – ($^2D^\circ$)$4p$ $^1F_3$	1.2e+08	D	9	C
881.393	0.006	113456.8	50	881.3978	0.0008[s]	($^2D^\circ$)$3s$ $^1D^\circ_2$ – ($^2D^\circ$)$4p$ $^1P_1$	1.5e+08	D	9	C
918.534	0.006	108869.1	50	918.5307	0.0007[s]	($^2D^\circ$)$3p$ $^3D_3$ – ($^2D^\circ$)$5s$ $^3D^\circ_3$	1.2e+08	D	9	C
925.038	0.006	108103.7	100	925.0456	0.0008[s]	($^4S^\circ$)$3p$ $^5P_1$ – ($^4S^\circ$)$5s$ $^5S^\circ_2$	8.1e+07	D	9	C
925.306	0.006	108072.4	160	925.3119	0.0008[s]	($^4S^\circ$)$3p$ $^5P_2$ – ($^4S^\circ$)$5s$ $^5S^\circ_2$	1.3e+08	D	9	C
925.760	0.006	108019.4	200	925.7654	0.0008[s]	($^4S^\circ$)$3p$ $^5P_3$ – ($^4S^\circ$)$5s$ $^5S^\circ_2$	1.9e+08	D	9	C
938.043	0.006	106604.9	30	938.0406	0.0008[s]	($^2D^\circ$)$3p$ $^3F_3$ – ($^2D^\circ$)$5s$ $^3D^\circ_2$	1.8e+08	D	9	C
938.454	0.006	106558.2	30	938.4544	0.0007[s]	($^2D^\circ$)$3p$ $^3F_4$ – ($^2D^\circ$)$5s$ $^3D^\circ_3$	1.8e+08	D	9	C
944.672	0.006	105856.8	50	944.6716	0.0004[s]	($^2D^\circ$)$3p$ $^1F_3$ – ($^2D^\circ$)$5s$ $^1D^\circ_2$	1.9e+08	D	9	C
1027.047	0.006	97366.5	140	1027.0439	0.0006[s]	($^4S^\circ$)$3s$ $^3S^\circ_1$ – ($^2P^\circ$)$3p$ $^3P_2$	3.9e+07	C	9	26
1027.521	0.006	97321.6	100	1027.5190	0.0006[s]	($^4S^\circ$)$3s$ $^3S^\circ_1$ – ($^2P^\circ$)$3p$ $^3P_1$	4.3e+07	C	9	26
1027.832	0.006	97292.2	50	1027.8318	0.0005[s]	($^4S^\circ$)$3s$ $^3S^\circ_1$ – ($^2P^\circ$)$3p$ $^3P_0$	4.5e+07	C	9	26
1035.695	0.006	96553.5	30	1035.6981	0.0006[s]	($^2D^\circ$)$3p$ $^3F_2$ – ($^2D^\circ$)$4d$ $^3G^\circ_3$	6.1e+07	D	9	C
1083.130	0.006	92325.0	30	1083.1150	0.0005[s]	($^2D^\circ$)$3p$ $^1D_2$ – ($^2D^\circ$)$5s$ $^1D^\circ_2$	1.4e+08	D	9	C
1093.030	0.006	91488.8	70	1093.0266	0.0009[s]	($^4S^\circ$)$3p$ $^3P_2$ – ($^4S^\circ$)$4d$ $^3D^\circ_3$	9.3e+07	D	9	C
1200.489	0.006	83299.4	90	1200.4839	0.0010[s]	($^4S^\circ$)$3p$ $^3P_1$ – ($^2D^\circ$)$3d$ $^3S^\circ_1$	5.7e+07	C	9	26
1200.638	0.006	83289.1	100	1200.6419	0.0011[s]	($^4S^\circ$)$3p$ $^3P_2$ – ($^2D^\circ$)$3d$ $^3S^\circ_1$	6.2e+07	C	9	26
1207.431	0.006	82820.5	100	1207.4201	0.0010[s]	($^4S^\circ$)$3p$ $^3P_1$ – ($^2D^\circ$)$3d$ $^3P^\circ_2$	2.3e+07	C	9	26

Table 2. *Continued.*

λ_{obs} (Å)[a]	Obs. unc.(Å)	σ_{obs} (cm^{-1})	Obs. int. and char.[b]	λ_{Ritz} (Å)	Ritz unc.[c](Å)	Transition[d]				A[e] (s^{-1})		Ref. λ[f]	Ref. A[g]
1207.575	0.006	82810.6	160	1207.5799	0.0010[s]	$(^4S^\circ)3p$	$^3P_2$ –	$(^2D^\circ)3d$	$^3P^\circ_2$	6.9e+07	C	9	26
1231.645	0.006	81192.2	180	1231.6461	0.0007[s]	$(^2D^\circ)3s$	$^3D^\circ_3$ –	$(^4S^\circ)4p$	$^3P_2$			9	
1232.101	0.006	81162.2	120	1232.0924	0.0008[s]	$(^2D^\circ)3s$	$^3D^\circ_2$ –	$(^4S^\circ)4p$	$^3P_2$			9	
1255.021	0.002	79679.92	240	1255.0186	0.0007[s]	$(^4S^\circ)3s$	$^3S^\circ_1$ –	$(^2D^\circ)3p$	$^3P_0$	1.2e+08	C	10	26
1255.691	0.002	79637.42	360	1255.6911	0.0007[s]	$(^4S^\circ)3s$	$^3S^\circ_1$ –	$(^2D^\circ)3p$	$^3P_1$	1.3e+08	C	10	26
1257.201	0.003	79541.8	500	1257.2070	0.0007[s]	$(^4S^\circ)3s$	$^3S^\circ_1$ –	$(^2D^\circ)3p$	$^3P_2$	1.3e+08	C	9	26
1375.023	0.002	72726.06	300	1375.0226	0.0008[s]	$(^2D^\circ)3p$	$^1P_1$ –	$(^2D^\circ)4s$	$^1D^\circ_2$	2.1e+08	D	10	C
1395.804	0.006	71643.3	50	1395.7970	0.0009[s]	$(^2D^\circ)3p$	$^3D_1$ –	$(^2D^\circ)4s$	$^1D^\circ_2$			9	
1448.193	0.006	69051.6	90	1448.2061	0.0009[s]	$(^2D^\circ)3p$	$^3D_1$ –	$(^2P^\circ)3d$	$^1D^\circ_2$	2.3e+05	C	9	26
1448.438	0.006	69039.9	200	1448.4368	0.0009[s]	$(^2D^\circ)3p$	$^3D_2$ –	$(^2P^\circ)3d$	$^1D^\circ_2$	1.3e+04	C	9	26
1449.899	0.006	68970.3	50	1449.8936	0.0009[s]	$(^2D^\circ)3p$	$^3D_3$ –	$(^2P^\circ)3d$	$^1D^\circ_2$	1.8e+05	C	9	26
1473.050	0.002	67886.36	360	1473.0495	0.0007[s]	$(^2D^\circ)3p$	$^1F_3$ –	$(^2D^\circ)4s$	$^1D^\circ_2$	3.4e+08	D	10	C
1499.364	0.009	66694.9	120	1499.3571	0.0010[s]	$(^2D^\circ)3p$	$^3F_2$ –	$(^2P^\circ)3d$	$^1D^\circ_2$	4.4e+05	C	9	26
1499.710	0.009	66679.6	180	1499.7045	0.0010[s]	$(^2D^\circ)3p$	$^3F_3$ –	$(^2P^\circ)3d$	$^1D^\circ_2$	2.3e+04	C	9	26
1508.343	0.009	66297.9	70	1508.3385	0.0010[s]	$(^2D^\circ)3p$	$^3F_3$ –	$(^2P^\circ)3d$	$^3F^\circ_2$	1.4e+06	C	9	26
1511.480	0.009	66160.3	160	1511.4740	0.0010[s]	$(^2D^\circ)3p$	$^3F_4$ –	$(^2P^\circ)3d$	$^3F^\circ_4$	1.1e+07	C	9	26
1570.733	0.009	63664.5	140	1570.7345	0.0009[s]	$(^2D^\circ)3s$	$^3D^\circ_3$ –	$(^2P^\circ)3p$	$^3P_2$	1.3e+06	C	9	26
1572.573	0.009	63590.1	90	1572.5732	0.0009[s]	$(^2D^\circ)3s$	$^3D^\circ_2$ –	$(^2P^\circ)3p$	$^3P_1$	8.1e+05	C	9	26
1573.806	0.009	63540.2	20	1573.8045	0.0009[s]	$(^2D^\circ)3s$	$^3D^\circ_1$ –	$(^2P^\circ)3p$	$^3P_0$	7.7e+05	C	9	26
1585.391	0.003	63075.92	400	1585.4013	0.0009[s]	$(^4S^\circ)3p$	$^3P_1$ –	$(^4S^\circ)4s$	$^3S^\circ_1$	3.3e+08	D	9	C
1585.655	0.003	63065.42	500	1585.6534	0.0010[s]	$(^4S^\circ)3p$	$^3P_0$ –	$(^4S^\circ)4s$	$^3S^\circ_1$	1.1e+08	D	9	C
1585.680	0.003	63064.43	500	1585.6768	0.0009[s]	$(^4S^\circ)3p$	$^3P_2$ –	$(^4S^\circ)4s$	$^3S^\circ_1$	5.5e+08	D	9	C
1604.734	0.002	62315.64	360	1604.7353	0.0005[s]	$(^2D^\circ)3s$	$^1D^\circ_2$ –	$(^2P^\circ)3p$	$^1D_2$	1.3e+08	C	10	26
1687.991	0.009	59242.0	140	1687.9944	0.0010[s]	$(^2D^\circ)3s$	$^3D^\circ_3$ –	$(^2P^\circ)3p$	$^3D_2$	2.8e+06	C	9	26
1688.776	0.003	59214.48	300	1688.7773	0.0011[s]	$(^2D^\circ)3s$	$^3D^\circ_3$ –	$(^2P^\circ)3p$	$^3D_3$	1.5e+07	C	9	26
1688.822	0.009	59212.9	260	1688.8327	0.0011[s]	$(^2D^\circ)3s$	$^3D^\circ_2$ –	$(^2P^\circ)3p$	$^3D_2$	1.1e+07	C	9	26
1689.374	0.009	59193.5	200	1689.3796	0.0011[s]	$(^2D^\circ)3s$	$^3D^\circ_1$ –	$(^2P^\circ)3p$	$^3D_1$	1.2e+07	C	9	26
1689.611	0.009	59185.2	100	1689.6164	0.0010[s]	$(^2D^\circ)3s$	$^3D^\circ_2$ –	$(^2P^\circ)3p$	$^3D_3$	1.9e+06	C	9	26
1839.729	0.009	54355.8	240	1839.7304	0.0011[s]	$(^2D^\circ)3p$	$^1D_2$ –	$(^2D^\circ)4s$	$^1D^\circ_2$	2.5e+08	D	9	C
1880.2095	0.0002	53185.562	240	1880.2095	0.0002[s]	$(^2P^\circ)3s$	$^1P^\circ_1$ –	$(^2P^\circ)3p$	$^1S_0$	6.8e+08	C	T	26
2065.3091	0.0002	48403.436	1000	2065.3090	0.0002[s]	$(^2D^\circ)3s$	$^1D^\circ_2$ –	$(^2D^\circ)3p$	$^1D_2$	4.7e+08	C	T	26
2088.889	0.009	47857.1	200	2088.8903	0.0009[s]	$(^2D^\circ)3p$	$^3D_1$ –	$(^2D^\circ)3d$	$^3D^\circ_2$	5.1e+07	C	9	26
2089.361	0.003	47846.31	300	2089.3706	0.0009[s]	$(^2D^\circ)3p$	$^3D_2$ –	$(^2D^\circ)3d$	$^3D^\circ_2$	2.8e+08	C	9	26
2149.8698	0.0004	46499.813	400	2149.8698	0.0004[s]	$(^2D^\circ)3p$	$^3D_2$ –	$(^2D^\circ)3d$	$^3F^\circ_3$	3.8e+08	C	T	26
2151.1999	0.0008	46471.06	300	2151.2003	0.0007[s]	$(^2D^\circ)3p$	$^3D_1$ –	$(^2D^\circ)3d$	$^3F^\circ_2$	3.6e+08	C	T	26
2153.085	0.009	46430.4	240	2153.0822	0.0006[s]	$(^2D^\circ)3p$	$^3D_3$ –	$(^2D^\circ)3d$	$^3F^\circ_3$	5.4e+07	C	9	26
2161.134	0.002	46257.47	800	2161.1350	0.0009[s]	$(^4S^\circ)3p$	$^5P_2$ –	$(^4S^\circ)3d$	$^5D^\circ_3$	4.3e+08	C	10	26
2163.7337	0.0003	46201.903	1000	2163.7337	0.0003[s]	$(^4S^\circ)3p$	$^5P_3$ –	$(^4S^\circ)3d$	$^5D^\circ_4$	6.4e+08	C	T	26
2176.6293	0.0003	45928.205	360	2176.6294	0.0003[s]	$(^2D^\circ)3s$	$^3D^\circ_1$ –	$(^2D^\circ)3p$	$^3P_0$	4.1e+08	C	T	26
2177.6980	0.0002	45905.669	400	2177.6980	0.0002[s]	$(^2D^\circ)3s$	$^3D^\circ_2$ –	$(^2D^\circ)3p$	$^3P_1$	3.0e+08	C	T	26
2178.6538	0.0003	45885.532	300	2178.6539	0.0003[s]	$(^2D^\circ)3s$	$^3D^\circ_1$ –	$(^2D^\circ)3p$	$^3P_1$	1.0e+08	C	T	26
2180.8631	0.0002	45839.052	600	2180.8631	0.0002[s]	$(^2D^\circ)3s$	$^3D^\circ_3$ –	$(^2D^\circ)3p$	$^3P_2$	3.4e+08	C	T	26
2182.2632	0.0003	45809.646	300	2182.2632	0.0003[s]	$(^2D^\circ)3s$	$^3D^\circ_2$ –	$(^2D^\circ)3p$	$^3P_2$	6.2e+07	C	T	26
2183.222	0.009	45789.5	120	2183.2231	0.0005[s]	$(^2D^\circ)3s$	$^3D^\circ_1$ –	$(^2D^\circ)3p$	$^3P_2$	4.1e+06	C	9	26
2197.789	0.009	45486.1	160	2197.7950	0.0010[s]	$(^2D^\circ)3p$	$^3F_3$ –	$(^2D^\circ)3d$	$^3D^\circ_2$	3.3e+07	C	9	26
2209.3151	0.0004	45248.789	400	2209.3151	0.0004[s]	$(^2P^\circ)3p$	$^3D_3$ –	$(^2P^\circ)3d$	$^3F^\circ_4$	6.1e+08	C	T	26
2211.8239	0.0005	45197.470	600	2211.8239	0.0005[s]	$(^2D^\circ)3p$	$^3F_2$ –	$(^2D^\circ)3d$	$^3G^\circ_3$	5.8e+08	C	T	26
2213.7211	0.0003	45158.739	800	2213.7210	0.0003[s]	$(^2D^\circ)3p$	$^3F_3$ –	$(^2D^\circ)3d$	$^3G^\circ_4$	5.8e+08	C	T	26
2263.1661	0.0006	44172.219	360	2263.1662	0.0006[s]	$(^2D^\circ)3p$	$^3F_4$ –	$(^2D^\circ)3d$	$^3F^\circ_4$	1.8e+08	C	T	26
2264.832	0.002	44139.73	320	2264.8351	0.0006[s]	$(^2D^\circ)3p$	$^3F_3$ –	$(^2D^\circ)3d$	$^3F^\circ_3$	1.6e+08	C	10	26
2273.5826	0.0003	43969.861	800	2273.5828	0.0003[s]	$(^2D^\circ)3p$	$^1F_3$ –	$(^2D^\circ)3d$	$^1G^\circ_4$	5.7e+08	C	T	26
2362.8647	0.0003	42308.576	300	2362.8645	0.0003[s]	$(^2P^\circ)3s$	$^3P^\circ_1$ –	$(^2P^\circ)3p$	$^3P_2$	7.9e+07	C	T	26
2363.2310	0.0002	42302.020	400	2363.2310	0.0002[s]	$(^2P^\circ)3s$	$^3P^\circ_2$ –	$(^2P^\circ)3p$	$^3P_2$	2.5e+08	C	T	26
2365.3821	0.0004	42263.553	260	2365.3822	0.0004[s]	$(^2P^\circ)3s$	$^3P^\circ_1$ –	$(^2P^\circ)3p$	$^3P_1$	8.7e+07	C	T	26

Table 2. *Continued.*

λ_{obs} (Å)[a]	Obs. unc.(Å)	σ_{obs} (cm^{-1})	Obs. int. and char.[b]	λ_{Ritz} (Å)	Ritz unc.[c](Å)	Transition[d]				A^e (s^{-1})		Ref. λ^f	Ref. A^g
2365.4188	0.0003	42262.897	280	2365.4187	0.0003[s]	$(^2P^\circ)3s$	$^3P^\circ_0$ –	$(^2P^\circ)3p$	$^3P_1$	1.1e+08	C	T	26
2367.0409	0.0003	42233.937	300	2367.0409	0.0003[s]	$(^2P^\circ)3s$	$^3P^\circ_1$ –	$(^2P^\circ)3p$	$^3P_0$	3.3e+08	C	T	26
2473.3862	0.0002	40418.188	600	2473.3862	0.0002[s]	$(^2P^\circ)3s$	$^1P^\circ_1$ –	$(^2P^\circ)3p$	$^1D_2$	2.7e+08	C	T	26
2589.9971	0.0003	38598.536	3000	2589.9970	0.0003[s]	$(^4S^\circ)3s$	$^5S^\circ_2$ –	$(^4S^\circ)3p$	$^5P_3$	2.4e+08	C	T	26
2593.5552	0.0003	38545.586	2500	2593.5551	0.0003[s]	$(^4S^\circ)3s$	$^5S^\circ_2$ –	$(^4S^\circ)3p$	$^5P_2$	2.4e+08	C	T	26
2595.6498	0.0003	38514.482	2000	2595.6498	0.0003[s]	$(^4S^\circ)3s$	$^5S^\circ_2$ –	$(^4S^\circ)3p$	$^5P_1$	2.4e+08	C	T	26
2611.409	0.002	38282.07	800	2611.4084	0.0006[s]	$(^2D^\circ)3s$	$^3D^\circ_3$ –	$(^2D^\circ)3p$	$^3F_3$	2.0e+07	C	10	26
2613.4161	0.0003	38252.674	2000	2613.4161	0.0003[s]	$(^2D^\circ)3s$	$^3D^\circ_2$ –	$(^2D^\circ)3p$	$^3F_3$	2.3e+08	C	T	26
2638.7112	0.0003	37885.999	1500	2638.7111	0.0003[s]	$(^2P^\circ)3s$	$^3P^\circ_1$ –	$(^2P^\circ)3p$	$^3D_2$	1.8e+08	C	T	26
2641.0831	0.0003	37851.976	1500	2641.0831	0.0003[s]	$(^2P^\circ)3s$	$^3P^\circ_2$ –	$(^2P^\circ)3p$	$^3D_3$	2.3e+08	C	T	26
2677.9047	0.0003	37331.535	2500	2677.9047	0.0003[s]	$(^4S^\circ)3s$	$^3S^\circ_1$ –	$(^4S^\circ)3p$	$^3P_2$	2.3e+08	C	T	26
2677.9717	0.0003	37330.601	1500	2677.9716	0.0003[s]	$(^4S^\circ)3s$	$^3S^\circ_1$ –	$(^4S^\circ)3p$	$^3P_0$	2.3e+08	C	T	26
2678.6912	0.0003	37320.575	2000	2678.6912	0.0003[s]	$(^4S^\circ)3s$	$^3S^\circ_1$ –	$(^4S^\circ)3p$	$^3P_1$	2.3e+08	C	T	26
2727.8987	0.0005	36647.401	240	2727.8985	0.0005[s]	$(^2D^\circ)3d$	$^1F^\circ_3$ –	$(^2D^\circ)4p$	$^1D_2$	9.2e+07	D	T	C
2766.9467	0.0005	36130.249	1500	2766.9467	0.0005[s]	$(^4S^\circ)3d$	$^3D^\circ_3$ –	$(^4S^\circ)4p$	$^3P_2$	1.4e+08	D	T	C
2777.6288	0.0003	35991.308	2500	2777.6288	0.0003[s]	$(^2D^\circ)3s$	$^3D^\circ_3$ –	$(^2D^\circ)3p$	$^3D_3$	1.8e+08	C	T	26
2785.2735	0.0004	35892.528	2000	2785.2734	0.0004[s]	$(^2D^\circ)3s$	$^3D^\circ_2$ –	$(^2D^\circ)3p$	$^3D_2$	1.4e+08	C	T	26
2787.6919	0.0005	35861.392	1500	2787.6919	0.0005[s]	$(^2D^\circ)3s$	$^3D^\circ_1$ –	$(^2D^\circ)3p$	$^3D_1$	1.4e+08	C	T	26
2866.7187	0.0005	34872.850	2500	2866.7190	0.0005[s]	$(^2D^\circ)3s$	$^1D^\circ_2$ –	$(^2D^\circ)3p$	$^1F_3$	1.9e+08	C	T	26

*In this shortened version of the table, only the lines selected as secondary Ritz standards are given.

[a]Observed wavelength is given in vacuum for lines shorter than 1999 Å and longer than 7000 Å. For the rest of the lines, observed wavelength is given in standard air. Conversion from vacuum to air was done using the five-parameter formula for refraction index of air from Peck and Reeder [27]. Symbol *p* in this column means that the line was predicted but not observed. Observed vacuum wave numbers were derived from the observed air wavelengths using the same formula of Peck and Reeder [27], except for the lines measured in the present work, for which the vacuum wave number was the primary measured quantity. Wave numbers of the lines from references [10,11] are cited from there.

[b]Line character legends (quoted from the references given in the last column): *w* – wide or diffuse or hazy; *c* – complex feature; *s* – shaded to shorter wavelengths; *l* – shaded to longer wavelengths; *bl* – blended with another line that may affect the wavelength and/or intensity; (includes "shoulder", "affected" etc.); *m* – masked by another line (no wavelength measured).

[c]An asterisk after the value of uncertainty of the calculated wavelength means that the upper or lower level of the transition is determined by this line alone. The uncertainties were determined by means of the LOPT code described in Appendix. Superscript *s* indicates that the Ritz wavelength of this line is suggested as a secondary wavelength standard.

[d]The parent term in parentheses refers to the $2s^22p^3$ configuration of the core. Question mark after the upper level means that identification of this level is questionable.

[e]The uncertainties of the transition probability values are denoted as follows: A – ≤3%; B – ≤10%; C – ≤25%; D – ≤50%.

[f]References to observed wavelengths and identifications. T means the present work.

[g]References to transition probabilities: 26 – the MCHF energy-adjusted transition probability data for Ne III were taken from the data collection of Froese Fischer and Tachiev [26] in the beginning of January 2004, just after they were re-calculated by Froese Fischer and Tachiev with corrected experimental energies from Persson [9]. Results of previous calculations posted on this website prior to that date used incorrect experimental energies, which caused errors up to a factor of two for several weak transitions; C – calculations with Cowan's codes, this work.

of 0.7 of their Hartree-Fock values and repeated the fitting. This time, the fitting converged with very small positive values of the α-parameters, indicating that the configuration interaction is now treated correctly. This procedure is equivalent to fixing the α-parameters at zero values and letting all CI parameters linked together to vary. However, the latter procedure requires much larger array dimensions and exhausts the available computer memory while leading to essentially the same results. The fitted parameters were used in Cowan's RCG code, producing improved transition probabilities. Then a separate utility program CONV_OUT was used to produce a simulated spectrum. This program reads output files of both RCG and Cowan's parametric fitting code RCE. Then it identifies the eigenvectors from the output file of RCE with those computed by RCG and substitutes the experimental levels from the RCE input file into transitions computed by RCG. The CONV_OUT code calculates relative intensities of the lines assuming Boltzmann level populations. An electron temperature 6 eV was assumed. All newly identified levels are located in the relatively narrow interval 483000 cm^{-1} to 535000 cm^{-1}, so the difference in collisional population rates in the plasma sources used in reference [13] (low-and high power Penning discharges)

should not lead to dramatic changes in relative intensities of lines, as compared with our calculations. Thus the predicted spectrum can be directly compared with the one observed by Livingston et al. [13]. In this way, the bulk of their list has been confirmed, with few exceptions. All of the new assignments made by Bastin [14] in Paul and Polster's line list [15] have also been confirmed.

Some of the multiple line assignments suggested in reference [13] were dropped from the list as these transitions have negligible transition probabilities compared to the other components of the same multiplet in the corresponding line blend. A few lines were supplemented with additional assignments to transitions that have a high calculated transition probability. The 208.9 Å and 219.6 Å lines, associated in reference [13] with the $2p^4\ ^3P_0$–$2p^3(^2P^\circ)4s\ ^3P^\circ_1$ and $2p^4\ ^1D_2$–$2p^3(^2P^\circ)4s\ ^1P^\circ_1$, probably arise from the previously unknown $2p^4\ ^1S_0$–$2p^3(^2P^\circ)5d^1P^\circ_1$ and $2p^4\ ^1S_0$–$2p^3(^2P^\circ)4d^1P^\circ_1$ transitions, which are predicted to be much stronger.

On the basis of the predicted wavelengths and relative line intensities, several previously unclassified lines below 208 Å were identified with high certainty as transitions from the previously unknown $2p^3(^4S^\circ)6d\ ^3D^\circ$, $2p^3\ (^4S^\circ)7d\ ^3D^\circ$, $2p^3(^2D^\circ)4d\ ^3D^\circ$, $^3S^\circ$, $^3P^\circ$ and $2p^3(^2P^\circ)4d\ ^1F^\circ$ terms.

We have also changed the identification of the blended 1810.13 Å line from the list of Persson et al. [9]. The $2p^3(^2D^\circ)3d\ ^3F^\circ_4 - 2p^3(^2D^\circ)4f\ ^1F_3$ intercombination transition is marked as "masked" because it has a very small transition probability, and a new assignment $2p^3(^2D^\circ)3d\ ^3F^\circ_3 - 2p^3(^2D^\circ)4f\ ^3F_4$ is added, which is predicted to be dominant in this blend.

8 Transition probabilities

Because of the astrophysical importance of the Ne III spectrum, transition probabilities of both allowed and reference transitions of this spectrum were extensively calculated by a number of authors. However, there have been only a few measurements of radiative lifetimes and transition rates.

Froese Fischer and Tachiev [26] have recently posted updated results on the World Wide Web for their energy-corrected multi-configuration Hartree-Fock (MCHF) calculations of Ne III. Where possible, we included their transition probabilities (A-values) in Table 2. Their uncertainty should be less than 25% in most cases. In a few cases, explained below, comparison with experimental data and other calculations justifies lower uncertainty estimates.

Using recent precise measurements of the radiative lifetime of the $2p^4\ ^1S_0$ level [28] we estimate that the uncertainty of the transition probabilities of the forbidden $2s^22p^4\ ^3P_1$–$2s^22p^4\ ^1S_0$ (magnetic dipole) and $2s^22p^4\ ^1D_2 - 2s^22p^4\ ^1S_0$ (electric quadrupole) transitions with Ritz wavelengths 1814.56 Å and 3342.18 Å is about 3%.

The uncertainty of the A-values for the magnetic dipole $2s^22p^4\ ^3P_1$–$2s^22p^4\ ^1D_2$ and $2s^22p^4\ ^3P_2$–$2s^22p^4\ ^1D_2$ transitions (observed at 3967.47 Å and 3868.76 Å, correspondingly) is less than 3%. This is confirmed by a very good agreement with results of Storey and Zeippen [29] and Galavis et al. [30].

The A-values for the far-infrared magnetic dipole transitions $2s^22p^4\ ^3P_2$–$2s^22p^4\ ^3P_1$ (15.5551 μm) and $2s^22p^4\ ^3P_1$–$2s^22p^4\ ^3P_0$ (36.0135 μm) calculated by different methods in references [26,31] (corrected for experimental energies) agree to within 2% and 5%, respectively. We consider these small differences as a measure of the uncertainties of these values.

Although, in general, calculations of Froese Fischer and Tachiev [26] are much more accurate than those of Bhatia et al. [25], the good agreement between them allows us to restrict the uncertainty bounds on the A-values to 10% for the $2s^22p^4\ ^3P$–$2s^22p^3(^2P^\circ)3d\ ^3P^\circ$, $2s^22p^4\ ^3P$–$2s^22p^3(^2D^\circ)3d\ ^3P^\circ$, $2s^22p^4\ ^3P$–$2s^22p^3(^2D^\circ)3d\ ^3D^\circ$, and $2s^22p^4\ ^1D$–$2s^22p^3(^2P^\circ)3d\ ^1F^\circ$ transitions in the VUV.

The A-values for the resonance transitions $2s^22p^4\ ^3P_{1,2}$–$2s2p^5\ ^3P^\circ_2$ agree to within 5% between the MCHF calculations [26] and earlier multi-configuration Dirac-Fock (MCDF) results [32]. However, the A-value for the intercombination transition $2s2p^5\ ^3P^\circ_2$–$2s^22p^3(^4S^\circ)3s\ ^5S^\circ_2$ reported in the MCHF data collection [26] is almost a factor of two lower than the MCDF result [32]. Although the MCHF result (cited from Ref. [26] in Tab. 2) should be more accurate, independent calculations of comparable quality are needed in order to confirm this value.

The transition probability of the $2s^22p^4\ ^1D_2$–$2s2p^5\ ^1P^\circ_1$ line at 379 Å given in reference [26] agrees very well with several other calculations summarized in reference [33]. However, the second, much weaker, decay branch of the same upper level, namely, the $2s^22p^4\ ^1S_0$–$2s2p^5\ ^1P^\circ_1$ transition at 428 Å, is much harder to calculate. For this line, results of several calculations reported in reference [33] are somewhat higher than the A-value in reference [26]. Several measurements of the 379/428 intensity ratio [34,35] also indicate that the A-value of the 428 Å line given in reference [26] may be too low by as much as 50%.

Although Cowan's programs [22] are very easy to use for calculations of transition probabilities, their results usually are not very accurate. Even if one uses Slater parameters adjusted by least-squares parametric fitting, the scope of included correlation effects is usually very limited. This approximation, as well as the limitation on the number of included configurations, makes it virtually impossible to obtain the same kind of accuracy with Cowan's codes as with the MCHF or MCDF codes that use multi-configuration basis wavefunctions. The accuracy of wavefunctions (and hence the A-values) computed by the latter two methods is much higher, because the radial parts of the basis wavefunctions are optimized in the variational procedure along with the expansion coefficients. However, we can expect the A-values computed by Cowan's codes to be rather accurate for transitions between almost pure states with no change of the core term or spin of the valence electron. For such LS-allowed

transitions, the low degree of state mixing implies little influence of configuration-interaction effects. Indeed, if we compare approximately 130 A-values computed by Cowan's codes [22] with reference [26] for transitions between the levels with 80% or higher purity of LS coupling, almost all of them agree to within 25% or less. Only four transitions have A-values that differ in Cowan's results and reference [26] by 30% to 35%, and one transition has a difference of 73%. This problematic transition is $2s^2 2p^3(^2\mathrm{D}^\circ)3p\ ^3\mathrm{P}_1 - 2s^2 2p^3(^2\mathrm{D}^\circ)3d\ ^3\mathrm{P}^\circ_1$ at 2460.725 Å. The lower and upper states are 93% and 99% pure in LS coupling, as calculated by Cowan's codes. Currently we cannot explain why the results of Cowan's codes and MCHF [26] differ so much for this transition. Nevertheless, we are still confident that, except for a few rare cases, transition probabilities of such LS-allowed transitions are calculated by Cowan's codes with uncertainties not exceeding 50%.

It should be taken into account that we speak here only about Cowan-code calculations using the Slater parameters substituted from the results of the least squares fitting of the known energy levels. Ab initio calculations using Cowan's codes produce energy levels that often deviate too much from the experimental ones. The error in transition energies, as well as the error in the degree of level mixing, can have an adverse effect on the transition probabilities.

With all precautions mentioned above, we selected the A-values computed by Cowan's codes that we expect to be accurate to within 50% and included them in Table 2 where MCHF results were not available.

9 Conclusion

As a result of the present work, 57 lines of Ne III have been precisely measured using Fourier transform spectroscopy. A comprehensive list of 824 emission lines of Ne III has been compiled. This line list includes more than a hundred lines for which the measurement uncertainty is significantly smaller than in the previous analysis done by Persson et al. [9]. About 80% of previously known energy levels of Ne III have been determined with improved accuracy. Over a hundred precise wavelength standards have been derived with well-defined uncertainties in the region 210 Å to 2900 Å. The value of the ionization potential of Ne III has been increased by 4.5 cm^{-1}. Nine new energy levels have been found, and 16 new transitions have been identified in the EUV range. Transition probabilities have been calculated and critically evaluated, and the best available value is given for approximately 70% of all lines.

The authors wish to express their gratitude to Dr. W.C. Martin for helpful discussions and making available some important sources of information, and to Dr. C. Sansonetti for numerous essential corrections to the manuscript and for permission to use his computer code for fitting the polarization formula. Dr. J. Reader provided a lot of valuable advice in preparation of the publication. This work was partly supported by the Office of Fusion Energy Sciences of the U.S. Department of Energy and by National Aeronautics and Space Administration.

Appendix: Level optimization program LOPT

This computer program was created at the National Institute of Standards and Technology in 1995 and was further developed in 1997–2003. Its name LOPT stands for Level Optimization. The basic method is a least squares fitting of the energy levels to the observed wave numbers that ideally should be exactly equal to the differences between the corresponding upper and lower levels. In this type of a problem, a sum of weighted squares of deviations is minimized. This minimization can be done either by iterations or by solving a set of linear differential equations by constructing and inverting a proper matrix of coefficients.

The program LOPT is written in Turbo-Pascal language for an IBM PC compatible computer. The basic algorithm implements the matrix inversion approach described by Radziemski et al. [36] and consists in the following.

The level-optimization problem can be formulated as minimization of the function F defined as

$$F = \sum_{i,j} (s_{ij} - \Delta E_{ij})^2 w_{ij}, \tag{4}$$

where s_{ij} is the measured wave number of the transition between the unknown energy levels E_i and E_j, $\Delta E_{ij} = E_i - E_j$, and the weight $w_{ij} = d_{ij}^{-2}$ is equal to the square of the reciprocal measurement uncertainty.

This leads to a set of linear equations of the form

$$\sum_j E_j W_{ij} = S_i, \tag{5}$$

where W_{ij} is a matrix of coefficients, and S_i are some combinations of s_{ij} and w_{ij} [36].

The solution is found by inverting the matrix W_{ij}:

$$E_j = \sum_i W_{ij}^{-1} S_i. \tag{6}$$

Apart from finding the optimized levels, the program LOPT calculates uncertainties of the predicted (Ritz) wave numbers. In the first version of the program we used an algorithm suggested by van het Hof in the appendix to his doctor thesis [37]. He introduced a concept of "error current", replacing the graph of energy levels connected by a set of observed transitions with an analogous electric circuitry. In this circuitry, transitions are replaced by resistances equal to squares of measurement uncertainties. In order to calculate relative uncertainty of any pair of levels, one should apply an arbitrary "voltage" between these levels and find the total "error current" between them. This will yield the total "resistance" between these two levels. The uncertainty of the energy difference (wave number of the transition) is equal to square root of this "resistance". In reference [37], this concept was applied only

to uncertainties of excited levels relative to the ground state, but the same procedure applies to any pair of levels. Thus, for each of the observed transitions, one needs to solve the problem of finding the "error currents" for each observed line separately, which implies inverting the corresponding matrix (each time different) as many times as there are observed lines. This demands a powerful computer. For Ne III, optimization of 250 energy levels against 900 observed lines could be easily performed even on an IBM-PC/386 computer within a few minutes of run-time whereas the computation of the uncertainties of predicted wave numbers takes several hours on a Pentium/90 computer. Although with modern desktop computers execution time is decreased by an order of magnitude, it is still considerable, especially for systems with larger numbers of energy levels.

Another algorithm of computation of the Ritz wavelength uncertainties, which has been finally implemented in the LOPT code, is based on the concept of covariance matrix developed by Radziemski et al. [36]. Using statistical theory, it can be rigorously shown that, if the wave number measurements s_{ij} are statistically independent, then the uncertainties a_{ij} of the energy differences $E_i - E_j$ are defined by a simple combination of the elements of the inverse matrix W^{-1}:

$$a_{ij} = \left(W_{ii}^{-1} + W_{jj}^{-1} - 2W_{ij}^{-1}\right)^{1/2}. \qquad (7)$$

This expression can be identified as the covariance matrix of the system (5). Using the relation (7), uncertainties of all Ritz wave numbers can be found after only one matrix inversion, and it is the same matrix that is used to determine the energy levels. This reduces the computation time by several orders of magnitude, compared with the "error current" algorithm. Numerical experiments showed that the results obtained with both algorithms are identical.

In references [36,37] it was noted that equations (4) through (7) are valid only if the measurements s_{ij} are statistically independent and have a normal distribution. It should be pointed out that, according to statistical theory [38], the assumption of a normal statistical distribution of measurements s_{ij} is not necessary for rigorous derivation of relations (5) through (7), provided that the individual terms in equation (4) are statistically independent. Thus, the requirement of the normal distribution of measurements is only significant for the validity of using weights inversely proportional to the square of measurement uncertainties in equation (4). If these measurement uncertainties are equal to the standard deviations of measurements, then the uncertainties a_{ij} defined by equation (7) also represent the standard deviations of the energy level differences derived from equation (6). The essential condition of the validity of these results is the *statistical independence* of the wave number measurements, i.e. absence of systematic errors.

Thus, the validity of both the "error current" and covariance-matrix approaches is restricted to the case of absence of systematic errors in the measured wave numbers. If some systematic errors are present, in certain cases they can result in progressive accumulation of systematic errors in the level values from the ground state to upper levels. The simplest example of this case is an almost equally spaced ladder-like level system for which the level values are derived from transitions occurring between the consecutive steps of the ladder. If all wave numbers of these transitions have a small systematic error in one direction, then the energy of the uppermost level relative to the ground level will have an error equal to the value of the systematic shift multiplied by the number of steps in the ladder. To our knowledge, there is no rigorous method developed for the estimation of level uncertainties caused by systematic errors in a general case.

Formula (7) was derived on the assumption that there is only one fixed level (the ground state) in the level system. Very often an atomic spectrum is divided into two or more independent sub-systems. For example, in the case of the Ne III spectrum, the quintet levels are not connected to triplet or singlet levels. In such cases, the usual way is to fix some additional levels in order to eliminate degeneracy of equation system (5). This fixing decreases the summation range in the left-hand side of equation (5) and modifies its right-hand side. As a consequence, although the levels still can be found from equation (6), the rigorous derivation that led to equation (7) cannot be followed in the same way. Thus, equation (7) becomes inapplicable. In addition, uncertainties of predicted intersystem lines cannot be derived because fixing of the levels assumes zero uncertainties. To avoid these difficulties, a concept of "virtually fixed levels" was introduced in the LOPT code. Instead of ultimately fixing the level, a *virtual transition* is added to the initial set of lines. This virtual transition connects the level with the ground state. The wave number of this transition is assumed to have a *finite* uncertainty. The whole problem is solved in two stages. In the first stage, the optimized levels are found, assuming the uncertainties of the virtually fixed levels to be very small. This effectively fixes these levels in the solution of equation system (5). In the second stage, the uncertainties of predicted wave numbers are found by solving the system (5) again, assuming some realistic (user-defined) uncertainties of the virtually fixed levels. The level values resulting from equation (6) in the second stage are ignored, as they could imply some deviation of the virtually fixed levels from their initial values, and this would lead to a shift of the levels that are directly connected to the virtually fixed levels by observed lines. So, in the second stage of solution, only the inverse matrix W^{-1} is found from equation system (5), and the uncertainties a_{ij} are determined using equation (7).

Another feature of the LOPT code is the possibility of determining the level values associated with unresolved blends of several transitions. This is done by multiplication of the line weights of the unresolved blend components by factors proportional to the calculated intensities:

$$w_{ij} = d_{ij}^{-2} I_{calc}/I_{tot}, \qquad (8)$$

where I_{tot} is the sum of the calculated intensities of all components of the blend. This is equivalent to multiplying the line uncertainties d_{ij} by the square root of the

corresponding reciprocal factors. Numerical experiments show that equation (8) results in correct optimized level values. A consequence of applying the additional weights in equation (8) is an increase of the uncertainties of the derived energy levels which is significant in the case when the upper level of the component transition in the blend is derived from this line alone. In such case, the uncertainty of the upper level increases exactly by the same factor equal to $(I_{tot}/I_{calc})^{-1/2}$ as the effective wave-number uncertainty of the line component. There is a pitfall in using the additional weights for components of blended lines occurring in the cases when the position of the line center is measured very precisely, e.g. with uncertainty that is much smaller than the distance between the positions of the components. In such cases, using the actual measurement uncertainty of the line in equation (8) would result in a distortion of the relative positions of the corresponding energy levels, since they would gravitate towards each other in order to reproduce the equal observed wave numbers of the component transitions. To avoid this effect, it is a rule of thumb to replace the actual measurement uncertainty of such precisely measured blends with a maximal separation between the line components or half of the line width, whichever is greater. A simple example of usage of blended lines in the level optimization is the unresolved $2p^3(^4\mathrm{S}^\circ)5f\ ^5\mathrm{F}$ term of Ne III which is connected to the well-resolved fine structure levels of the $2p^3(^4\mathrm{S}^\circ)3d\ ^5\mathrm{D}^\circ$ term by one blended line at 1295.57 Å. If this were the only line defining the upper term, it would be simple to use the individual components of the unresolved multiplet to derive the fine-structure components of the upper ^{5}F term and then find the center of gravity of the term. However, there is also another blended line at 3921.03 Å connecting this term with the $2p^3(^4\mathrm{S}^\circ)4d\ ^5\mathrm{D}^\circ$ term which is also resolved. Having this additional connection greatly complicates the problem of finding the center of gravity of the ^{5}F term because of the various measurement uncertainties that should enter into the averaging procedure. The program LOPT makes such problems very easy to solve by using equation (8).

Some lines can be excluded from the level-optimization procedure by setting a corresponding flag ("masked" or "predicted") in the input file. For these lines, the program finds the Ritz wavelengths and their uncertainties.

Although it was mentioned above that there is no way to rigorously estimate the effect of the possible systematic errors on the derived energy levels, a reasonable estimate still can be provided for certain types of systematic shifts. In the LOPT code, the following algorithm is used to estimate systematic shifts that can be represented as uniform displacements of certain groups of lines relative to each other. The list of observed spectral lines is divided into several groups. In each group K, all lines are supposed to be correlated, i.e. it is assumed that all measured wave numbers between states E_i and E_j in the group are affected by the same value of systematic shift δ_K:

$$s_{ijK} = s^*_{ijK} + \delta_K, \tag{9}$$

where s^*_{ijK} represents the unshifted wave number.

The smallest uncertainty of the measured wave number in the group is adopted as the upper bound of this group's possible systematic shift δ_K. This assumption is reasonable for most types of spectral measurements. For example, in the case of grating or prism spectrometers, the usual procedure is to form a polynomial calibration curve of the spectrometer. This calibration curve is obtained by fitting the measured positions of a set of reference lines. The standard deviation of this fit is included in the measurement uncertainties of the lines. The errors in the positions of the reference lines represent a common source of the systematic shift. Obviously, the smallest quoted line-measurement uncertainty must have the largest contribution of these systematic errors to the total uncertainty. Similarly, for FTS measurements the smallest quoted uncertainties have a negligible contribution of the statistical uncertainty and the largest contribution of the residual uncertainty $\delta\sigma_r$ (see Sect. 2) that represents the systematic error. This assumption is not rigorously justified in all cases, but it provides a reasonable estimate of the group shift δ_K. The effect of this shift on the level energy E_j resulting from the solution of the least-squares problem can be estimated by differentiating equation (6) with respect to the group-shift variable δ_K. The derivative is simple since the inverse matrix W^{-1} does not depend on wave numbers (it is a combination of reciprocal squared uncertainties), and the variables S_i depend on the measured wave numbers linearly. The calculated derivative multiplied by the estimated upper bound of systematic shift δ_K is an estimate of the possible error in level energy due to this systematic shift.

Thus, for each energy level, apart from the usual standard deviation of the calculated energy, we have a set of additional possible errors due to systematic shifts of each group of correlated lines. If the level is determined from several lines, these shifts must be added to the standard deviation in order to obtain a more confident estimate of the possible error. The program LOPT does this adding by computing the square root of the sum of squares of the standard deviation and all estimated uncertainties due to systematic line-shifts. The only exception is the case of a level determined by a single line. In this case no adding is done, as the estimated standard deviation of such level coincides with the wave-number measurement uncertainty, which already includes the possible systematic error.

The effect of the possible systematic error of a certain group of lines on the calculated wave numbers is estimated in the same manner, by computing the derivative of each calculated wave number on the group-shift variable and multiplication of this derivative by the upper-bound estimate of this group shift. The squares of the contributions from each line group are added to the square of the standard deviation to obtain the square of the estimated uncertainty of the calculated wave number, except for the case when this line alone determines one of the two levels involved.

Using this estimate of the possible effect of systematic shifts in the program LOPT alleviates the problem of accumulation of systematic errors in the derived energy

levels. For the above-mentioned simple case of an equally-spaced ladder-like system of levels, the uncertainty of the uppermost level resulting from the LOPT code would naturally include the effect of accumulation of the error. It has no effect on the values of level energies and Ritz wave numbers but increases the resulting uncertainties.

To run the program, the user needs to create three input files: the file of transitions, the file of fixed levels, and the parameter file. The latter provides a detailed description of the format of the first two files and various other settings required to run the code. The transition and fixed-level files are simple ASCII text files in which the data are arranged in fixed-width columns. In the current version of the code, the number of transitions is limited to 10000 and the number of levels to 1000. There is no limitation on the type of transitions. They can be either "allowed" or "forbidden", which means that they can have both levels of the same parity. Inclusion of such forbidden transitions was a problem for some other level-optimization programs.

The program is available from the author at `Alexander.Kramida@nist.gov`. The code is still under development. However, complete user documentation is available along with the source code. The full text of the program will be published in a separate publication when translation into C++ language is completed.

References

1. T.L. de Bruin, Z. Phys. **77**, 505 (1932)
2. V. von Keussler, Z. Phys. **85**, 1 (1933)
3. J.C. Boyce, Phys. Rev. **46**, 378 (1934)
4. C.E. Moore, NBS Circ. 488, Sec. I, 78 pp. (1950)
5. I.S. Bowen, Astrophys. J. **121**, 306 (1955)
6. I.S. Bowen, Astrophys. J. **132**, 1 (1960)
7. W. Persson, Phys. Scripta **3**, 133 (1971)
8. B. Edlén, Phys. Scripta **22**, 593 (1980)
9. W. Persson, C.-G. Wahlström, L. Jönsson, H.O. Di Rocco, Phys. Rev. A **43**, 4791 (1991)
10. J. Sansonetti, J. Reader, C. Sansonetti, N. Acquista, J. Res. Natl. Inst. Stand. Technol. **97**, 1 (1992)
11. H. Feuchtgruber, D. Lutz, D.A. Beintema, E.A. Valentijn, O.H. Bauer, D.R. Boxhoorn, Th. De Graauw, L.N. Haser, G. Haerendel, A.M. Heras, R.O. Katterloher, D.J.M. Kester, F. Lahuis, K.J. Leech, P.W. Morris, P.R. Roelfserna, A. Salama, S.G. Schaeidt, H.W.W. Spoon, B. Vandenbussche, E. Wieprecht, Astrophys. J. **487**, 962 (1997)
12. J.W. Brosius, R.J. Thomas, J.M. Davila, Astrophys. J. **526**, 494 (1999)
13. A.E. Livingston, R. Büttner, A.S. Zacarias, B. Kraus, K.-H. Schartner, F. Folkmann, P.H. Mokler, J. Opt. Soc. Am. B **14**, 522 (1997)
14. T. Bastin, thèse de docteur en science, Université de Liége (1996)
15. F.W. Paul, H.D. Polster, Phys. Rev. **59**, 424 (1941)
16. G. Nave, S. Johansson, A.P. Thorne, J. Opt. Soc. Am. B **14**, 1035 (1997)
17. G. Nave, S. Johansson, R.C.M. Learner, A.P. Thorne, J.W. Brault, Astrophys. J. Suppl. Ser. **94**, 221 (1994); J. Sugar, C.H. Corliss, J. Phys. Chem. Ref. Data Suppl. **14**, 1 (1985); M. Rosberg, S.G. Johansson, Phys. Scripta **45**, 590 (1992); E. Biémont, S. Johansson, P. Palmeri, Phys. Scripta **55**, 559 (1997)
18. J.W. Brault, Mikrochim. Acta (Wien) **III**, 215 (1988)
19. G. Norlén, Phys. Scripta **8**, 249 (1973)
20. W. Whaling, W.H.C. Anderson, M.T. Carle, J.W. Brault, H.A. Zarem, J. Quant. Spectrosc. Radiat. Transf. **53**, 1 (1995)
21. G. Nave, C. Sansonetti, J. Opt. Soc. Am. B **21**, 442 (2004)
22. R.D. Cowan, *The theory of atomic structure and spectra* (University of California Press, Berkeley, Los Angeles, London, 1981)
23. P.J. Mohr, B.N. Taylor, *The 2002 CODATA Recommended Values of the Fundamental Physical Constants, Web Version 4.0,* available at `http://physics.nist.gov/constants` (National Institute of Standards and Technology, Gaithersburg, MD 20899, 9 December 2003); P.J. Mohr, B.N. Taylor, Rev. Mod. Phys. **77**, 1 (2005)
24. R.J. Thomas, W.M. Neupert, Astrophys. J. Suppl. Ser. **91**, 461 (1994)
25. A.K. Bhatia, R.J. Thomas, E. Landi, At. Dat. Nuc. Data Tables **83**, 113 (2003)
26. C. Froese Fischer, G. Tachiev, *The MCHF/MCDHF Collection*, `http://atoms.vuse.vanderbilt.edu/`
27. E.R. Peck, K. Reeder, J. Opt. Soc. Am. **62**, 958 (1972)
28. E. Träbert, A. Wolf, X. Tordoir, E.H. Pinnington, E.J. Knystautas, G. Gwinner, A.G. Calamai, R.L. Brooks, Can. J. Phys. **79**, 145 (2001)
29. P.J. Storey, C.J. Zeippen, Mon. Not. R. Astr. Soc. **312**, 813 (2000)
30. M.E. Galavis, C. Mendoza, C.J. Zeippen, Astron. Astroph. Suppl. Ser. **123**, 159 (1997)
31. G. Gaigalas, J. Kaniauskas, R. Kiselius, G. Merkelis, M.J. Vilkas, Phys. Scripta **49**, 135 (1994)
32. C. Froese Fischer, X. He, P. Jönsson, Eur. Phys. J. D **4**, 285 (1998)
33. M.J. Vilkas, G. Merkelis, R. Kisielius, G. Gaigalas, A. Bernotas, Z.B. Rudzikas, Phys. Scripta **49**, 592 (1994)
34. E. Träbert, H.-P. Garnir, P.D. Dumont, T. Bastin, Eur. Phys. J. D **15**, 25 (2001)
35. H.-J. Flaig, K.-H. Schartner, E. Träbert, P.H. Heckmann, Phys. Scripta **31**, 255 (1985)
36. L.J. Radziemski Jr, K.J. Fisher, D.W. Steinhaus, Comp. Phys. Comm. **3**, 9 (1972)
37. G.J. van het Hof, *Orthogonal operators in atomic 3d systems*, Academisch Proefschrift ter verkrijging van de graad van doctor aan de Universiteit van Amsterdam, 1990
38. V.N. Vapnik, T.G. Glazkova, V.A. Koshsheyev, A.I. Mikhalskii, A. Ya. Chervonenkis, *Algorithms and Programs for Reconstruction of Dependencies* (Nauka, Moscow, 1984)